2011

Investigation of Crumb Rubber Concrete for Blast Protection of Buildings

Joseph Charles States
Lehigh University

Investigation of Crumb Rubber Concrete for Blast Protection of Buildings

By

Joseph States

A Thesis

Presented to the Graduate and Research Committee

of Lehigh University

in Candidacy for the Degree of

Master of Science

In

Structural Engineering

Lehigh University

April, 2011

This thesis is accepted and approved in partial fulfillment for the requirements of the Master of Science in Structural Engineering.

_____

Date

_____

Dr. Clay Naito

Thesis Advisor

_____

Dr. Stephen Pessiki

Department of Civil & Environmental Engineering

Acknowledgements

This research was conducted at the Air Force Research Laboratories at Tyndall AFB, Panama City, FL, USA and at the University of Missouri. Funding for the research was provided by the Air Force Research Laboratories. The experiments were designed and conducted by Dr. Clay Naito[1], Christopher Jackson[2], and Bryan Bewick[3]. Their work is gratefully acknowledged. Publications regarding this research are pending to the ASCE Structural Journal and the International Journal of Impact Engineering.

I would like to thank my thesis advisor, Dr. Clay Naito, for his mentorship and guidance throughout my master's studies. The computer and technical support provided by Peter Bryan was invaluable. Thanks are extended to my fellow graduate students for the assistance and support in both technical and nontechnical challenges throughout my studies. Finally, I want to thank my family and friends for their support.

[1] Associate Professor. Department of Civil and Env. Engrg., Lehigh University ATLSS Center, 117 ATLSS Dr., Bethlehem, PA 18015, USA, Email: cjn3@lehigh.edu, Phone: 610-758-3081, Fax: 610-758-5553.

[2] Air Force Research Laboratory Support Contractor, Applied Research Associates, Inc., Tyndall AFB, FL, USA.

[3] Research Civil Engineer, Air Force Research Laboratory, Tyndall AFB, Panama City FL, 32403, USA.

Table of Contents

List of Figures

List of Tables

Abstract

To address the ever increasing quantity of scrap tires produced in the U.S. a study is conducted on the use of crumb rubber in concrete for enhancement of structures against blast effects. Crumb Rubber Concrete (CRC) is produced by replacing a volume percentage of the traditional coarse and/or fine aggregate with crumb rubber particles. Crumb rubber is produced in various gradations from used vehicle tires. Part 1 of the research program characterizes the mechanical properties of CRC and provides an assessment of the capability of CRC in providing flexural resistance against blast effects. Part 2 of the research study examines the use of CRC for the specialized application of blast and ballistic protection. The program characterizes resistance of CRC to contact and near contact high explosive detonations, and examines depth of penetration, and perforation using V50 methods.

The results of part 1 of the experimental and analytical investigation found that (1) crumb rubber replacement of coarse and fine aggregate is done at a cost premium of approximately ¾ times the replacement percentage, (2) the addition of crumb rubber results in a decrease in unit weight, compression strength, splitting tensile strength, and elastic modulus, linearly related to the addition of rubber, (3) the modulus of rupture was not sensitive to up to 40% rubber aggregate replacement, and (4) flexural failure modes occur at lower demand levels for due to the use of rubber replacement. The reductions are in line with the material property conclusions previously discussed.

The results of part 2 of the experimental and analytical investigation found that (1) the addition of crumb rubber results in decreased resistance to ballistic demands and near-field blast loads, (2) the reduction is less than that expected by accepted predictor methods and (3) when normalized by weight rather than thickness, the addition of CRC results in an improvement in resistance to ballistic and near-field blast demands.

Chapter 1: Introduction

One of the most problematic sources of waste produced in the United States is scrap tires. Based on 2003 statistics, it has been estimated that the U.S. produces 290 million waste tires annually, with over 265 million in stockpiles [EPA 2008]. Such a large grouping of tires provides fire and health hazards. Since they are harmful, very bulky and mostly void space, dumping whole tires in landfills has been banned in 38 states [EPA 2008]. As an alternative to discarding whole tires, they can be taken to tire shredding processors where the tires can be reduced to smaller pieces known as tire chips or crumb rubber [Eldin 1993]. The pieces can then be burned, stored in landfills, or used as a construction material [Taha 2008]. Shredded tire bits are only used sparingly in construction since rubber does not provide any significant structural qualities. The most common use of, waste rubber, more specifically tire chips, have been in highway asphalt mixes. This process has been well documented and used in practice since 1990 [Epps 1994 and Khatib 1999]. Extending this concept for Portland cement concrete mixes has gained interest in recent years. To accomplish this, portions of coarse and fine aggregate are replaced with tire chips and crumb rubber, respectively.

Material characterization experiments have been conducted to determine the practicality of using crumb rubber in Portland cement concrete. Research has shown that replacement of conventional aggregates with rubber results in a decrease in compressive and tensile strength and stiffness. Eldin and Senouci [1993] performed tension and compression tests on two types of cylinders, with portions of the coarse or fine aggregate

replaced with rubber. They observed tensile strength decreases of 50% and compression strength reductions of up to 85% however noted that the rubberized concrete absorbed a great amount of plastic energy. Khatib and Bayomy [1999] observed similar behavior and recommended a practical limit of 20% volumetric replacement of aggregate to maintain reasonable structural performance.

The use of rubber aggregate in Portland cement concrete has shown to improve the energy absorbing characteristics. Turatsinze et al. [2005] observed that the rubber acts as a crack arrester. When the cracks meet the rubber particles, the rubber absorbs the cracking stresses. This increases the strain capacity prior to macro-cracking. Therefore, it was concluded that when strength is not a limiting factor, rubberized concrete may be used to resist cracking. Further research conducted by Taha et al. [2008] on the micro-structure of the crumb rubber indicated that tire chips increase the fracture toughness and impact resistance of the concrete. The rubber acts as an additional energy absorber that toughens the concrete. Zheng et al. [2008] tests concluded that the brittleness index is reduced with the addition of rubber aggregate. This signified a greater ductility in the rubberized concrete. Wong and Ting [2009] performed experiments on normal and high strength rubberized concrete and found that the rubberized concrete exhibited less brittle failure and higher energy absorption capacity.

Based on the published literature on crumb rubber concrete (CRC) it is apparent that ductility and energy absorption is enhanced over that of conventional concrete. These characteristics may prove beneficial for applications where dynamic blast pressure demands are a concern.

1.1 Research Significance

Due to our military presence in hostile territories worldwide, personnel in military facilities are recurrently subjected to blast, fragmentation, and ballistic threats. One such threat that must be considered in these situations is that of a mortar attack. Mortar detonations on or near the roof or exterior walls of a building can cause damage to structure as well as the occupants. Damage is generated as a result of both the explosive pressure demands and the impact of fragments. Fragmentation of mortar casing produces high velocity low mass projectiles which can penetrate or perforate concrete wall and roof elements. Concrete materials are also known to fracture and spall when subjected to near-field blast. This can create high velocity fragmentation hazards that can cause extensive collateral damage to the very assets they are designed to protect.

While it has been generally accepted that rubber significantly decreases the overall strength of concrete, previous research has indicated that rubberized concrete has improved energy absorption over traditional concrete. In this research program, the constitutive properties of CRC are closely examined for a variety of rubber replacements. The goal is to determine if these properties can provide enhanced flexural response protection against blast detonation at moderate to large standoffs. The flexural performance of wall panels fabricated from CRC is experimentally examined and the predictive response against blast demands is evaluated.

Additionally, the brittle mode response of CRC to close-in blasts and ballistics is directly examined for a variety of rubber replacements. The goal of the research program is to

determine if CRC provides enhanced resistance over conventional concrete and to examine if conventional predictor methods can be used to estimate the performance.

Chapter 2: Mechanical Properties and Flexural Performance of CRC

2.1 CRC Mix Development

The CRC used in the experimental program was chosen to produce designs with mechanical properties acceptable for building construction. The quantity of coarse and fine rubber aggregates was limited to a 40% volume replacement of the aggregate. Rubber replacements in excess of 40% result in excessive decreases in strength and stiffness and were not included.

The mix constituents included Type 1 cement, crushed coarse aggregates, natural fine aggregates, and crumb rubber. A crushed limestone with a #67 coarse aggregate gradation (0.75 in. (19.0 mm) to No.4) was used for coarse aggregate. A standard natural sand gradation was used for the fine aggregate in accordance with ASTM C33. The crumb rubber aggregate was produced from shredded scrap tires. The majority of remnant tire materials including steel and dust were removed. The crumb rubber was produced using ambient techniques (shredded at room temperature). This method is different from conventional techniques which cryogenically process and shred the material. The ambient technique was chosen to minimize the effect of the shredding on

the mechanical properties of the rubber. Coarse crumb rubber (CCR) and fine crumb rubber (FCR) were used in the research program. A #5 CCR gradation (9.5 - 6.4 mm) with a bulk weight of 34.0 lb/ft^3 (0.54g/cm^3) was used for the coarse aggregate replacement. A #2 FCR gradation (passing a No.5 to No.10 sieve) with a bulk weight of 28.40 lb/ft^3 (0.45 g/cm^3) was used for the fine aggregate replacement. The coarse and fine crumb rubber aggregates and the typical distribution of rubber in the concrete are illustrated in **Error! Reference source not found.**.

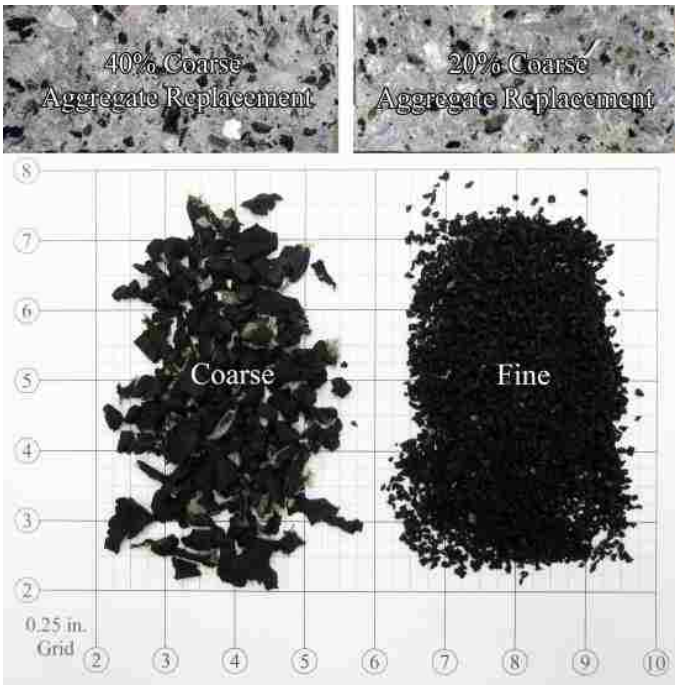

Figure 1: Rubber aggregates and distribution in cracked sections

2.1.1 CRC Mix Properties

CRC mixes were fabricated with variations in the amount of rubber aggregate as summarized in Table 1. Mix design was based on a standard 4000 psi (27.60 MPa)

strength target using an absolute volume basis design. Rubber replacement levels were made relative to the volume of coarse and fine aggregate replaced. The volumetric aggregate replacement percentage refers to the volume of coarse or fine stone aggregate replaced by rubber. The volumetric rubber replacement represents the percentage of volume of rubber compared to the total volume of concrete batched. The design water to cement ratio, unit weight, air content, and slump measurements were recorded for the majority of batches and are presented in Table 1.

Table 1: Batch Matrix and Properties

ID	Volumetric Aggregate Replacement		Rubber Volume per Total Volume	Water Cement Ratio	Unit Weight [lb/ft^3] (kg/m^3)	Slump [mm]	Air [%]
	Coarse	Fine					
A-10-10-.40	10%	10%	6.4%	0.40	-	-	-
A-20-10-.40	20%	10%	10.0%	0.40	-	-	-
A-20-10-.45	20%	10%	10.0%	0.45	-	-	-
A-40-10-.45	40%	10%	17.3%	0.45	-	-	-
Control	0%	0%	0.0%	0.40	-	-	-
A1-20-0-.40	20%	0%	7.3%	0.40	140(2242)	178	3.4
A1-20-10-.40	20%	10%	10.0%	0.40	134(2147)	64	5.0
A1-40-0-.40	40%	0%	14.5%	0.40	132(2115)	102	3.5
A1-40-10-.40	40%	10%	17.3%	0.40	124(1986)	76	6.0
Control II	0%	0%	0.0%	0.40	153(2451)	140	2.0
A2-20-0-.40	20%	0%	7.3%	0.40	143(2291)	83	3.0
A2-40-0-.40	40%	0%	14.5%	0.40	132(2115)	203	4.0
Control III	0%	0%	0.0%	0.52	150(2403)	127	2.0

Rubber aggregate replacement results in a direct decrease in unit weight and an increase in the air content as illustrated in Figure 2. The decrease in unit weight is linearly related to the addition of rubber aggregate. Given that the rubber has a considerably lower density than the stone aggregate the volumetric replacement results in a proportional decrease in the unit weight. The increase in air content with rubber content can be

roughly approximated with a linear relationship. The air content measurements ranged from 3% to 4% in batches incorporating only CCR. Conversely, batches incorporating both FCR and CCR ranged from 5% to 6%. This may be due to the fact that the FCR particles are hydrophobic, and create miniscule rivulets around the particles. These rivulets may form air pockets during the hydration process. Another likely possibility is that unlike all the other concrete constituents, the rubber particles are compressible. This compressibility would result in an artificial amount of air using standard ASTM C231 Test Methods. The air quality should be examined further through a study of the hardened air properties.

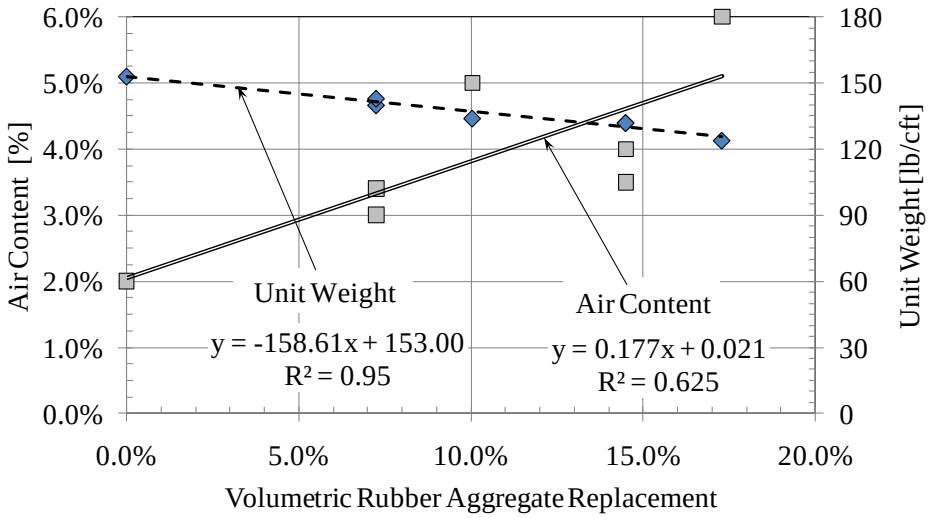

Figure 2: Influence of rubber content on air content and unit weight [1 lb/ft^3=16 kg/m^3]

2.2 Mechanical Properties of CRC

The mechanical properties of CRC were assessed in accordance with ASTM specifications. The compressive strength, tensile strength, modulus of rupture, elastic modulus, and stress-strain characteristics were determined. The variation in performance is compared with percentage replacements of stone coarse and fine aggregates with crumb rubber aggregates, and control mix designs containing no crumb rubber aggregate. When applicable the performance is compared with commonly accepted formulations of strength and response.

2.2.1 Compressive Strength

The strength gain for the cylinders was measured using 102 mm diameter 203 mm tall cylinders in accordance with ASTM C39. The cylinders were stored submerged in lime saturated water until testing in accordance with ASTM C192. The compressive strength reduction relationship at an age of 28-days is illustrated in Figure 3. The strength reduction is linearly proportional to the volumetric quantity of rubber, $R_{\%Vol}$, used in the concrete.

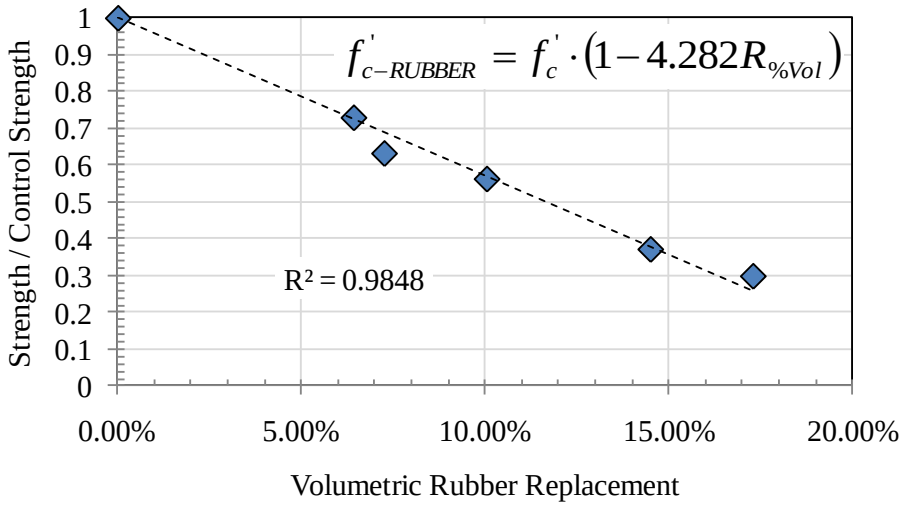

Figure 3: 28-day strength reduction with rubber addition

The strength gain with time is illustrated in Figure 4. The amount of coarse crumb rubber replacement directly influences the compressive strength. The strength decrease is consistent at the 7-day, 21-day, and 28-day ages. The reduction in the compressive strength is proportional to the rubber quantity.

The strength gain data is fit to ACI 209R [1992] compressive strength gain formulations. The fit is illustrated in Figure 4. The formulation has the form of equation 1. The regression fit of the data for parameters α and β are presented in Table 2. Based on accuracy of the regression, the 10% and 20% coarse aggregate replacement regressions provide a good fit to the data. The 40% replacement however does not.

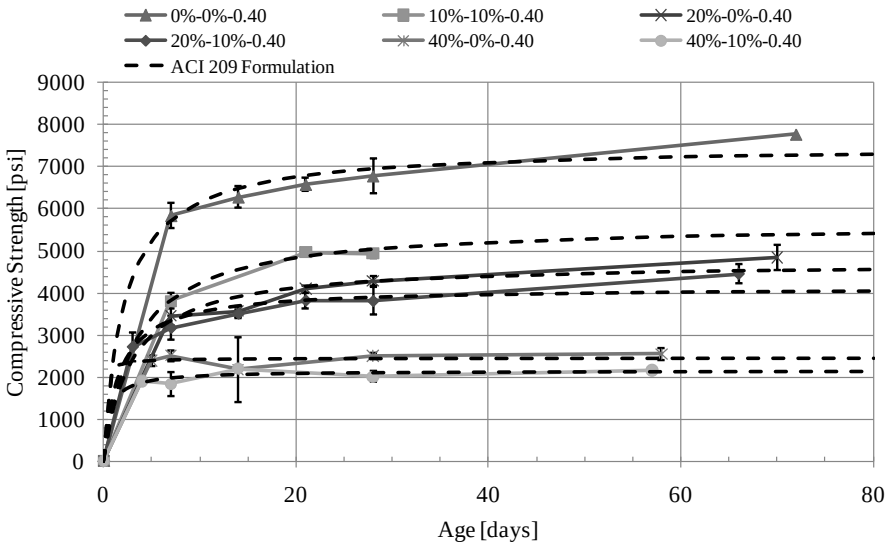

Figure 4: ACI 209 estimated strength gain [1 psi = 6.89 kPa]

$$f'c(t) = \frac{t}{\alpha + \beta \cdot t} f'c_{28-Days} \quad [units: t - days] \qquad Equation\ 1$$

Table 2: Long-term strength gain			
Mix	α	β	R^2
0%-0%-0.40	1.985	0.905	0.846
10%-10%-0.40	2.921	0.877	0.987
20%-0%-0.40	2.642	0.908	0.803
20%-10%-0.40	1.529	0.925	0.911
40%-0%-0.40	0.128	1.023	0.020
40%-10%-0.40	0.562	0.939	0.475

Splitting Tensile Strength

The tensile strength of CRC was measured in accordance with ASTM C496. The results are tabulated in Table 3. Splitting tensile strength of concrete, f'_t, is assumed to be proportional to the square root of the compressive strength, f'_c. The commonly accepted relationship for tensile strength for normal strength and weight concrete (Equation 2) is

valid for low rubber replacement levels but is not representative of higher levels of replacement.

$$f'_t = 6.0\sqrt{f'c} \quad \textit{units: [psi] or} \quad f'_t = 15.75\sqrt{f'c} \quad \textit{units: [kPa]} \qquad \textit{Equation 2}$$

Table 3: Tensile strength

Mix Design	f'_c [psi(MPa)]	f'_t [psi(kPa)]	f'_t #sqrt(f'_c)
10%C-10%F-0.40	4940 (34.06)	421 +/- 14 (2902 +/-96)	6.00 (15.7)
20%C-10%F-0.40	3967 (27.35)	360 (2481)	5.72 (15.0)
40%C-10%F-0.40	1468 (10.12)	176 +/- 32 (1213 +/-220)	4.59 (12.1)
20%C-10%F-0.45	3678 (25.36)	343 (2365)	5.66 (14.8)
40%C-10%F-0.45	2490 (17.17)	222 +/- 14 (1530 +/196)	4.45 (11.7)

The splitting tensile strength decreases as a function of the coarse aggregate replacement. For higher aggregate replacements the splitting strength of the material decreases with respect to the square root of the compressive strength. An estimate of the decrease of tensile strength with respect to the percentage of coarse aggregate replacement, *C*, is presented in Figure 5.

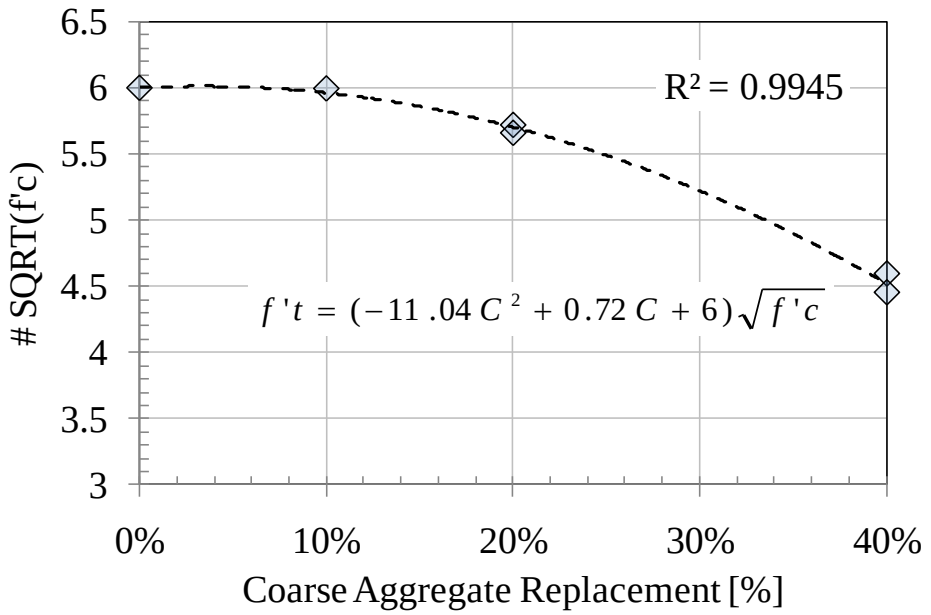

Figure 5: Splitting tension strength reduction with coarse aggregate replacement [Units: f'_c (psi)]

2.2.2 Flexural Tensile Strength – Modulus of Rupture

The modulus of rupture (MOR) of CRC was measured in accordance with ASTM C78. The measured MOR for the five mix designs are presented in Table 4. Modulus of rupture of concrete, f'_r, is commonly computed with respect to the square root of the compressive strength, f'_c. The relationship for normal strength and weight concrete (equation 3) is conservative for all rubber replacement levels except for the 40%C-10%F case. The absolute rupture strength consistently decreases with the addition of rubber aggregate; however, this effect is not present when normalized by the compressive strength. The addition of fine rubber aggregate does not consistently alter the strength.

$$f'r = 7.5\sqrt{f'c} \text{ units: [psi] or } f'r = 19.69\sqrt{f'c} \text{ units: [kPa]} \qquad \text{Equation 3}$$

Table 4: Modulus of rupture and elastic properties [1 psi = 6.89 kPa]						
Crumb Rubber Replacement	Average f'_r, [psi]	f'_c [psi]*	$\#\ of\ \sqrt{f'c}$	Average Modulus of Elasticity [ksi]	Peak Stress [psi]	Strain at Peak Stress
0%C-0%F	718	8218	7.91	5777±831	7905±311	2.08E-03
20%C–0%F	530±55	5122	7.40	5030±558	4525±393	1.33E-03
20%C-10%F	523±45	4531	7.77	3663±474	4042±235	1.48E-03
40%C-0%F	414±24	2563	8.18	3454±738	3088±19	1.42E-03
40%C-10%F	307±27	2180	6.58	2612±133	2525±14	1.57E-03

2.2.3 Constitutive Properties

CRC mix designs were examined to determine the variation in elastic properties with changes in rubber aggregate replacement including elastic modulus, peak stress, and strain at peak stress. Testing was done in accordance with ASTM C469 and is summarized in Table 4.

The compressive elastic modulus of CRC decreases with increases in quantity of rubber aggregate. The elastic modulus of rubber is significantly lower than that of hardened concrete. Consequently, under compressive loads the rubber aggregate performs as a void in the concrete. The elastic properties can be approximately scaled from that of standard concrete by accounting for the loss in concrete volume or weight resulting from the rubber replacement.

The elastic modulus of CRC is compared with two formulations. The first accounts for the change in unit weight, w_c, and the compressive strength of the material. This method is based on ACI 318 recommendations for elastic modulus of concrete as noted in equation 4.

$$E_{c1} = w_c^{1.5}\ 33 f'^{0.5}_c \text{ units: } [lb/ft^3 \text{ and psi}] \qquad \text{Equation 4}$$

The second formulation is based on the total reduction in aggregate content. This method uses the percentage replacement of aggregate (as opposed to the volumetric replacement) as presented in equation 5.

$$E_{c2} = E_{c\ Control}\ x\ (1 - \%\ Agg.Replacement) \qquad \textit{Equation 5}$$

The accuracy of the two relationships is illustrated in Figure 6. The ACI formulation results in only a 4% error for the control mix but underestimates the elastic modulus of all CRC mixes by over 10%. The volumetric reduction method provides a better estimate of the elastic modulus with an error of 10% or less. The second method (Equation 5) is recommended.

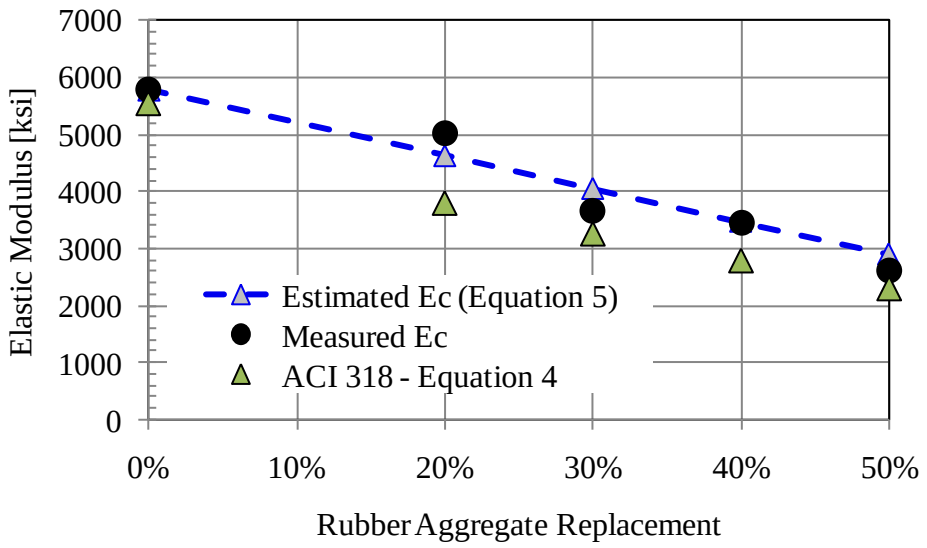

Figure 6: Relationship between elastic modulus and rubber aggregate (1ksi = 6.894MPa)

2.3 Flexural Performance of CRC

The flexural performance of CRC was examined to determine if the strength or deformation capability of the material would provide enhancements over traditional concrete. The study focuses on the performance of standard wall panels used as exterior cladding on building systems. The panels examined replicate precast walls used in non-load bearing façade applications. The panels were designed for wind and handling loads. Each panel was reinforced at the center with conventional reinforcement for flexural demands and temperature and shrinkage requirements. The panels measure 12 ft (3657.6mm) long and 6 in. (152.4mm) thick. The panels were tested in one-way action over a 10 ft (3048mm) span and were subjected to a uniform load. A width of 16 in. was examined, due to the one-way action of the panel the performance is representative of similar panels of greater width. The panel details are illustrated in Figure 7.

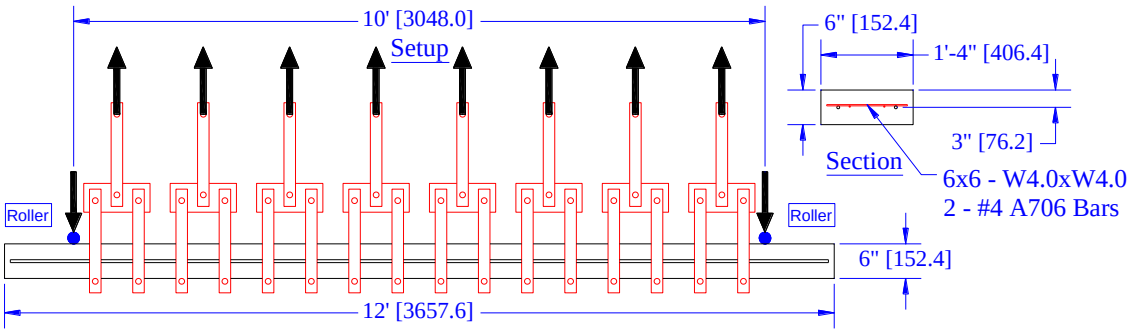

Figure 7: Panel section and loading setup

Each panel was loaded using a standard loading tree test fixture as illustrated in Figure 7 and was tested under a quasi static displacement control until failure. The load and displacements for each test were measured. The load is reported with respect to the uniform pressure applied to the 10ft (3048mm) tested span of the panel. Displacements

were measured at midspan. The panels were load tested at the University of Missouri [Bewick et. al. 2010]. Three concrete types were evaluated: a control batch, a 20% coarse aggregate replacement, and a 40% coarse aggregate replacement. For each concrete type three experiments were performed. Further details on the performance of each panel can be found in Bewick et al., 2010.

The quantity of WWR and the depth to the reinforcement varied between specimens. The average depths and reinforcement areas were measured after each test. The compression strength was measured in accordance with ASTM methods. The strength was measured twice, first at 28 days and again at 90 days within two weeks of the uniform loading tests. Due to the age of the panels the compression data taken at 90 days is assumed to be representative of the final panel material strength. The modulus of rupture and elastic modulus were approximated using the formulations developed in previous sections. As-built properties as well as estimated material properties for each slab type are in Table 5.

Table 5: Material properties of panel specimens

Mix	Approximate Compressive Strength [psi]	*Estimated* f'_r [psi]	*Estimated* E_c [ksi]	Unit Weight [lb/ft^3]	Average rebar depth from tension face [in.]	Average WWR depth from tension face [in.]	Total Area of WWR [in^2]
0%	5559 +/- 152	559	4656	153	2.83	2.45	0.11
20%	3557	447	3725	143	2.65	2.18	0.12
40%	2793 +/- 193	396	2793	132	2.65	2.18	0.08

As an example, the full results for the 20% replacement are presented in Figure 8. A comparison of the average responses for the three concrete types is illustrated in Figure 9. The total history is presented as well as the elastic region shown on the inset. The average as-built properties for each concrete type are not exactly the same so direct comparison is limited to a discussion of the cracking and stiffness performance. The max pressure, P_{max}, corresponding displacement, Δ_{max}, elastic stiffness, and cracking pressure, P_{cr} are summarized in Table 6. The cracking strength, ultimate strength, ultimate displacement, and elastic stiffness decrease with rubber replacement.

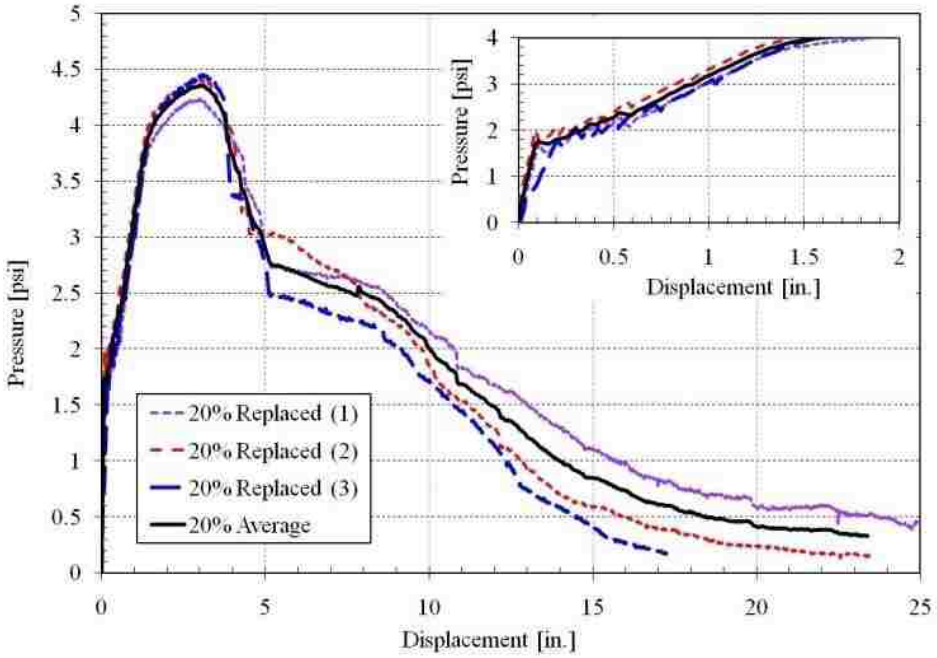

Figure 8: Pressure – deformation response 20% rubber aggregate (1psi = 6.894 kPa, and 1in = 2.54cm)

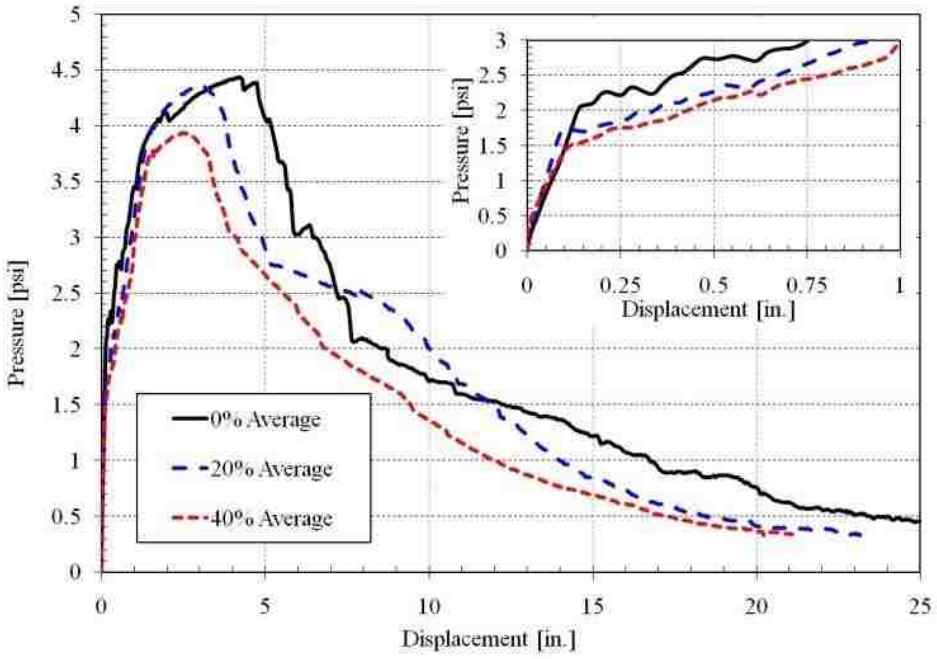

Figure 9: Average pressure – deformation response (1psi = 6.894 kPa, and 1in = 2.54cm)

Table 6: Average measured response				
CRC type	P_{cr} [psi]	Elastic Stiffness, [psi/in]	P_{max} [psi]	Δ_{max} [in.]
0%	2.34±0.28	16.95±4.2	4.41±0.22	3.60±1.45
20%	1.83±0.15	14.53±5.0	4.37±0.11	3.05±0.05
40%	1.56±0.12	10.40±3.5	3.96±0.16	2.72±0.24

2.3.1 Estimate of Response Based on Mechanical Characteristics

Measured and estimated responses of the uniform loading test are compared to assess the accuracy of the estimation methods. Estimated load-deflection curves are created using tas-built properties and material characteristics presented in Table 5. A simplified tri-linear moment-curvature analysis was conducted using the limit states of cracking, yield,

and nominal strength. Ultimate deflection was found at each limit state using standard integration methods.

The cracking moment was estimated using strength of materials in accordance with Equation 6. The cracking moment, M_{cr}, is related to the panel thickness, t, the gross moment of inertia, I_g, and the modulus of rupture, f'_r.

$$M_{cr} = f'_r \, x \, I_g / (t/2) \qquad \textit{Equation 6}$$

The yield strength was estimated using the Hognestad stress-strain model for the compressive concrete [1951]. The distance to the neutral axis, c, was found by integrating the compressive stress from the Hognestad equation, equation 7, and setting this concrete compressive force equal to the force of reinforcement at yielding. Given the value of c, the moment was found by integrating the stress multiplied by the distance to the reinforcement from the neutral axis to the ultimate compressive fibers. The steel was assumed to have a yield strength of 80 ksi (552 MPa), and an elastic modulus of 29000 ksi (199948 MPa).

$$\sigma(\varepsilon) = f_c^{'}\left(\frac{2\varepsilon}{\varepsilon_0} - \left(\frac{\varepsilon}{\varepsilon_0}\right)^2\right) \qquad \textit{Equation 7}$$

The nominal strength was estimated in accordance with ACI 318 [2008] procedures, equation 8. The nominal moment, M_n, is related to cross-sectional area of rebar and WWR, A_s and A_{wwr}, the stress in the rebar and WWR, f_s, the width of panel, b, and the Whitney stress block depth, a, and the depth to reinforcement, d.

$$M_n = (A_s + A_{WWR}) * f_s * (d - a/2) \qquad \textit{Equation 8}$$

$$a = \frac{(A_s + Awwr) * fs}{0.85 f_c' b}$$

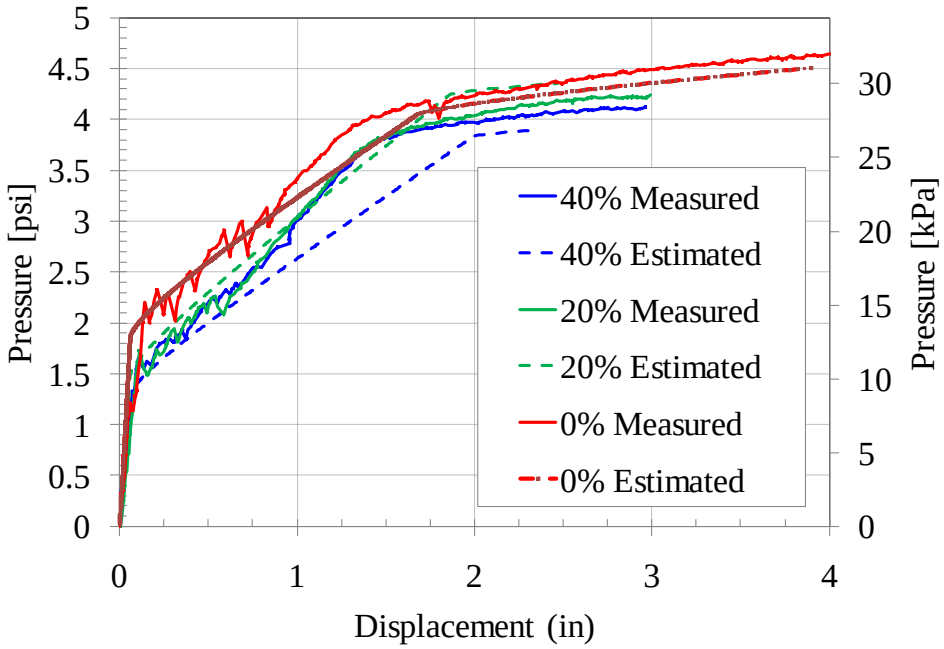

Figure 10: Measured and theoretical pressure displacement curves

Figure 10 compares the theoretical values with the measured resistance functions. The theoretical curves represent the as-built conditions and are terminated at the nominal capacity. The theoretical graphs for the 0% and 20% provide an accurate fit of the measured response. The 40% case resulted in a good fit of the elastic and cracking behavior and a conservative estimate of the post cracking response.

2.3.2 Estimated Dynamic Enhancements Provided by CRC

The theoretical resistance functions can be used to provide a prediction of the dynamic response under an exterior explosion. The responses of the CRC panels are estimated using single degree of freedom modeling techniques as described in detail in Biggs [1964]. The panel is simplified to a single degree of freedom spring-mass system. The resistance of the spring is based on the pressure – displacement response provided in Figure 10. The panel unit weight is accounted for. The panels are assumed to span 10 ft (3048mm) and are simply supported. The panels are assumed to form a flexural yield mechanism at midspan.

Concrete models with 0% and 40% CRC were directly compared using the same cross-section. The cross section, illustrated in the inset of Figure 11, has a height of 6 in, width of 16 in, and 0.5 in^2 of steel reinforcement with yield strength of 75 ksi (517 MPa) at mid-height. Additionally, a second cross section was modeled with 40% CRC that included a height of 7 in with the same reinforcement also at mid-height. The second cross-section with 40% CRC is approximately the same weight as the original cross-section with 0% CRC. In this way 40% and 0% CRC concrete are compared for an identical reinforcement detail and for a section of equal weight. The displacement time history response to a blast demand with a peak positive reflected pressure of 27.3 psi and positive impulse of 121 psi-msec is shown in Figure 11. The peak responses are summarized in Table 7.

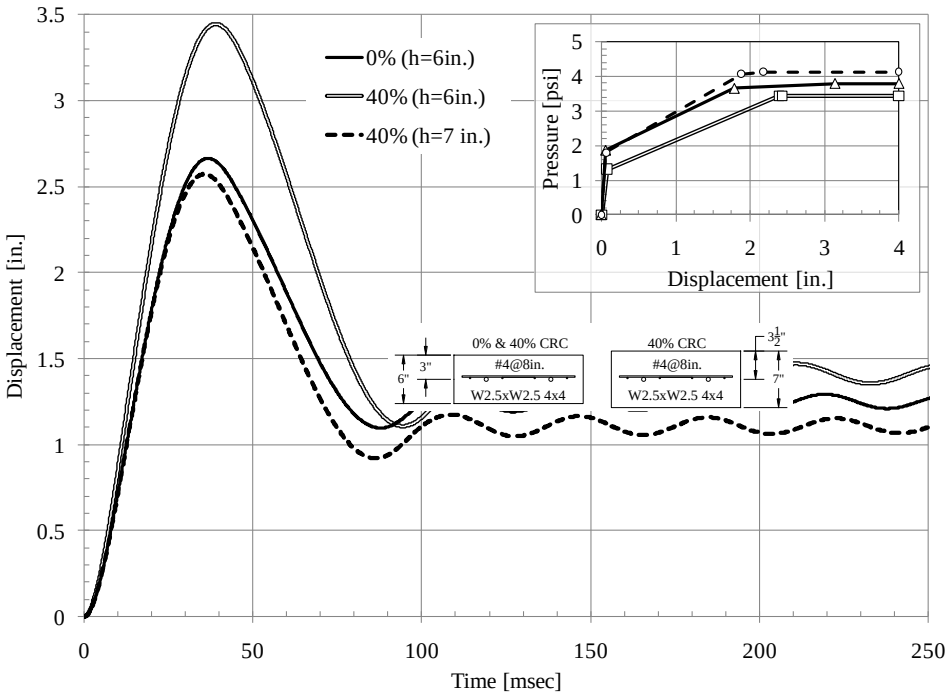

Figure 11: Displacement time history for CRC panels subject to blast demand (1 in = 2.54 cm)

Table 7: Estimated displacement under blast demands

% Coarse Aggregate Rubber Replacement	Max Displacement [in.(cm)]	Increase relative to 0%	Permanent Displacement [in.(cm)]	Increase relative to 0%
0%, 6 in. depth	2.66(6.76)	100%	1.25(3.17)	100%
40%, 6 in. depth	3.44(8.81)	129%	1.40(3.56)	112%
40%, 7 in. depth	2.57(6.53)	97%	1.11(2.82)	89%

The 0% CRC experiences a significantly smaller displacement than the 40% CRC for an identical section. However the analysis shows that for a section of similar weight, the 40% CRC material can be used to achieve less peak and permanent displacement than the 0% CRC section.

2.4 Cost Implications of Using CRC

The use of crumb rubber in concrete is accomplished by replacement of low cost coarse and fine aggregates. Consequently, rubber replacement is done at a premium as illustrated in Figure 12. The cost estimates were conducted in December 2009. The cost of ambient rubber is $0.37 per kg while coarse and fine aggregates are priced at $0.04 per kg and $0.02 per kg, respectively. Due to the low cost for stone aggregates, rubber additions are not significantly offset by the reduction in conventional aggregates. Estimated cost per cubic yard for different rubber contents were calculated by utilizing the specific gravity and batching ratios used in this research program. A baseline concrete cost of $100 per cubic yard ($76 per cubic meter) is assumed for this example. An increase in rubber coarse aggregate results in a proportional (approximately 0.75) increase in the cost. For example a 40% addition of rubber results in roughly a 30% increase in cost. This is reduced for fine aggregate replacements due to the fact that fine aggregate represents a smaller portion of the concrete volume. For CRC to be economical, the performance benefits must outweigh the additional cost.

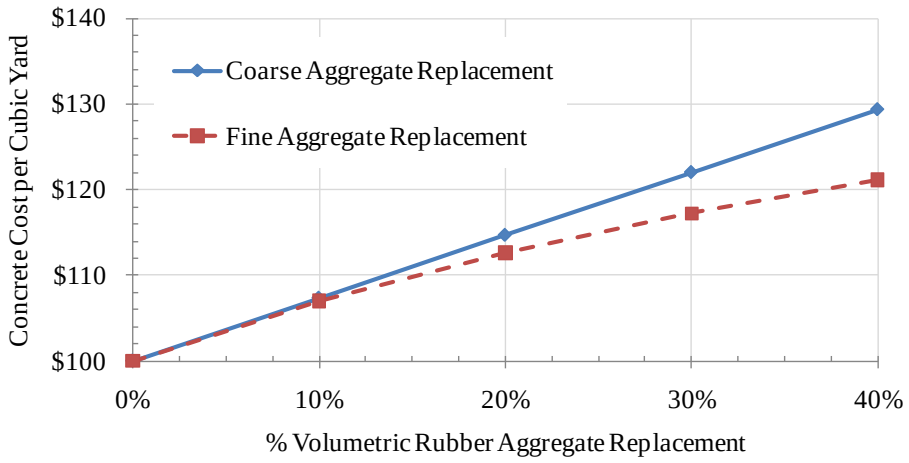

Figure 12: Cost premium for crumb rubber additions [1 yd^3 = 0.76 m^3]

2.5 Conclusions and Recommendations

An experimental study was conducted to assess the mechanical characteristics of Portland cement based concrete fabricated with shredded rubber aggregate. Variations in coarse and fine aggregate replacements were examined and used to assess the practicality of using the material for blast resistant applications. The following conclusions can be drawn from the research presented.

- The unit weight of CRC decreases linearly with the addition of rubber aggregate. The decrease is directly related to the low specific gravity of the rubber (1.03). Since the rubber has a considerably lower density than the stone aggregate the volumetric replacement results in a proportional decrease in the unit weight. A formulation for estimating unit weight from the rubber content was developed.

- The plastic air content increases with the rubber content. Also, the batches incorporating fine crumb rubber had higher air content values. This may be due to the fact that the FCR particles are possibly somewhat hydrophobic, thus creating miniscule rivulets around the particles. These rivulets may form air pockets during the hydration process. Another likely possibility is that unlike all the other concrete constituents, the rubber particles are compressible. This compressibility would result in an artificial amount of air using standard ASTM Test procedures.
- The use of ambient crumb rubber in concrete is accomplished at a cost premium. Utilizing the specific gravity and batching ratios an increase in rubber coarse aggregate was found to produce a proportional (approximately 0.75) increase in the cost. For example a 40% addition of rubber results in roughly a 30% increase in cost. This is reduced for fine aggregate replacements due to the fact that fine aggregate represents a smaller portion of the concrete volume. For rubber concrete to be economical the performance benefits must outweigh the additional cost.
- The compressive strength of concrete decreases with the replacement of rubber aggregate. The reduction in the compressive strength is linearly proportional to the volumetric quantity of rubber used in the concrete. A formulation for estimating the strength reduction based on the volumetric rubber replacement was developed and found to provide a good fit.
- The ACI 209 formulations for strength gain were found to provide a good estimation of strength for CRC with rubber replacements of 20% or less. The 40% mix was not predicted well by the ACI formulations.

- The tensile splitting strength of CRC was found to decrease with the addition of rubber. The decrease is expected since under tension the rubber aggregate acts as voids in the concrete thus decreasing the gross cross-section of the concrete. A second degree relationship between splitting tension strength, rubber content and compressive strength was developed and found to provide an accurate prediction. The addition of rubber aggregate does not significantly alter the flexural tensile strength (modulus of rupture, MOR) of the material when normalized by the compressive strength.
- The elastic modulus of CRC decreases with the addition of rubber. The reduction in elastic modulus is found to be accurately modeled by accounting for the percent volumetric replacement of rubber. A 20% replacement of rubber would result in a 20% decrease in elastic stiffness. The volumetric reduction method provides an error of 10% or less.
- As expected, based on the material characteristics, the flexural cracking strength, ultimate strength, ultimate displacement, and elastic stiffness decrease with an increase in rubber aggregate replacement.
- The pressure displacement curve was modeled using a moment-curvature analysis. The model fits fairly closely with the measured data for 0%, 20%, and 40% replacement.
- The blast resistance of CRC decreases with the addition of rubber. When the size of a specimen with 40% CRC is normalized to have the same weight as a specimen with 0%CRC, the maximum displacements of the 40% CRC specimen experiences less maximum and permanent deflection.

In summary the use of CRC decreases strength, stiffness, and flexural resistance of concrete. This is directly attributed to the addition of the rubber which has a low mass and strength relative to the other constituents used in concrete. The low mass however results in a decrease in unit weight when rubber aggregate is used. When accounting for the weight of the material the same dynamic flexural response and level of protection can be achieved with an equivalent weight of CRC material. The use of CRC however is done at a cost premium due the high relative cost of crumb rubber over traditional concretes. For building systems requiring large areas of protection the weight savings would provide reduced dead load on the building. For this particular example, the cost savings in a smaller gravity system may outweigh the added cost of CRC over traditional concrete.

Utilizing the material strength reductions developed in this research CRC can be safely used for military and government facilities where blast or ballistic threats are expected. This should only be conducted if the design goal is to dispose of vehicle tires in a safe manner, otherwise the cost of using CRC will likely be a premium to the construction project.

Chapter 3: Near Field Blast and Ballistic Performance of CRC

3.1 CRC Properties

Mechanical property tests were completed prior to the ballistic tests. Compressive strength tests were completed in accordance with ASTM C39 on 4x8 cylinders stored in accordance with ASTM C31. Tensile concrete strength tests were completed in accordance with ASTM C496 or ASTM C78. ASTM C496 provides a measure of the pure tensile strength of concrete while C78 provides a measure of tension strength in the presence of flexure. The Batch Matrix and Properties are presented in Table 1.

As discussed previously, volumetric replacement of stone based aggregates with crumb rubber results in a decrease in unit weight, a decrease in compressive strength, and a decrease in tensile strength. No significant change in the modulus of rupture was observed when normalized with respect to the square root of the compressive strength. The materials used in this study are in line with those observations.

Table 8: Batch Matrix and Properties [1 psi = 6.894 kPa]							
Study	Volumetric Aggregate Replacement		Volumetric Rubber Replacement	Unit Weight [lb/ft^3] (kg/m^3)	Compressive Strength, f'_c [psi]	Tension Strength [psi]	Tension Strength [#sqrt(f'c)]
	Coarse	Fine					
Spall and Breach	0%	0%	0.0%	-	5559 +/- 152	-	-
	20%	0%	7.3%	143(2291)	3557 +/- NA	-	-
	40%	0%	14.5%	132(2115)	2793 +/- 193	-	-
Ballistic Penetration	10%	10%	6.4%	-	4940 +/- 99	421+/-14[1]	6.00
	20%	10%	10.0%	-	3967 +/- 34	360[1]	5.72
	40%	10%	17.3%	-	1468 +/- 135	176+/-32[1]	4.59
Ballistic Perforation	0%	0%	0.0%	153(2451)	8195[2]	394[3]	7.72
	0%	0%	0.0%	153(2451)	3365 +/- 144	493[3]	6.91
	20%	0%	7.3%	140(2242)	5100[2]	662[3]	7.31
	40%	0%	14.5%	132(2115)	2610[2]	424[3]	7.31

[1]Tension strength measured by splitting tension test on cylinder in accordance with ASTM C496.

[2]Compression strength is estimated from strength gain measured in accordance with ASTM C39.

[3]Tension strength measured by modulus of rupture in accordance with ASTM C78.

3.2 Spall/Breach of CRC

The spall and breach capacity of CRC was examined to evaluate if the resistance is affected by the amount of crumb rubber aggregate present in the concrete. Due to the low stiffness and apparent energy absorbing characteristics of CRC the performance under spall and breach conditions is assessed. The spall and breach characteristics were compared to the performance of traditional concretes as predicted by methods outlined in the Unified Facility Criteria 3-340-02 [2008].

Close-in detonation of high explosives produces a high velocity pressure wave that in turn creates shock wave propagation through solid wall elements. The shock wave initiates as a compression wave which is reflected as a tension wave when it hits the back face of the panel. If the resulting stress from the sum of the tension wave and

compression wave exceeds the tensile capacity of the concrete spalling occurs [UFC 3-340-02 2008].

Due to the short duration over which the shock wave transmission occurs and the acceleration of the wall itself, spalled pieces of concrete can have a velocity of several hundred feet per second as they separate from the wall producing a danger for occupants of the structure. When the spall depth exceeds half the depth of the wall breaching typically occurs [US Army 1998]. Breaching provides an added danger to the occupants since it allows for insertion of small arms into the protected space.

3.2.1 Spall and Breach Experiment Design

Three mix designs were examined: a control (no rubber), a 20% coarse aggregate replacement, and a 40% coarse aggregate replacement. Compressive strength of the concrete was determined within 1-day of the detonation. The properties of the three concrete mixes are summarized in Table 1. The strength of the concrete decreased linearly with volumetric addition rubber aggregate.

Three panels were fabricated using each concrete mix. The panels were sized to have a surface width and length greater than twice the predicted spall diameter. The panel dimensions are illustrated in Figure 13. A low level of reinforcement was used to ensure integrity of the slab prior to testing without significantly influencing the spall and breach characteristics. Welded wire reinforcement (6 in. x 6 in. W4.0 x W4.0 meeting the requirements of ASTM A185) was placed at the mid-depth of the panel. This reinforcement provided a gross reinforcement ratio of 0.0011, which is less than 0.0014,

the ACI 318 [2008] requirement for temperature and shrinkage reinforcement of slabs. The spall and breach detonations were conducted with the panels in a horizontal orientation. Each panel was supported on four edges using a wooden frame resting on a sand base. Approximately 2.5 in. (64 mm) of the outer panel edge was supported on the wood frame (Figure 13).

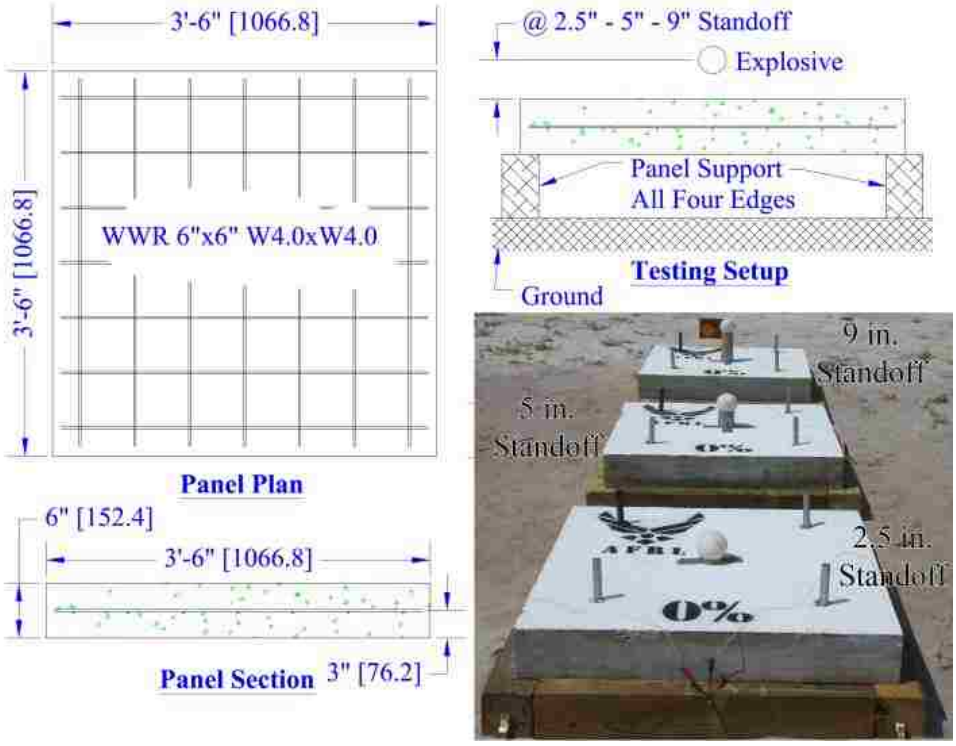

Figure 13: Spall and breach setup (1 in = 2.54 cm)

Each concrete type was examined under three blast demands. The panels were exposed to an identical charge, at three different stand-off distances. The explosive used in this experiment was 2.0 lbs. (0.907 kg) of C-4 molded into a sphere approximately 4 in. (100 mm) diameter. The stand-off distances were 2.5 in., 5.0 in., and 9.0 in. (63.5 mm, 127 mm, 228.6 mm) measured from the panel face to the center of the charge. The three C-4

spheres for each concrete type were detonated simultaneously to minimize the effect on the adjacent panel. The panel layout for the control concrete just prior to detonation is illustrated in Figure 13.

3.2.2 Spall and Breach Results

Following detonation the panels were examined for spall and breach damage on the front and rear faces. The resulting damage to each panel is presented in Figure 14. The images present the front and rear face damage for each panel. As illustrated the 2.5 in. (63.5 mm) standoff resulted in breach of all panels, while the 5 in. (127 mm) standoff produced spall on the interior face and the 9 in. (228.6 mm) standoff only produced spall on the 20% aggregate replacement specimen. The average measured spall diameter on the front and rear face and the diameter of the breach, if present, are summarized in Table 9.

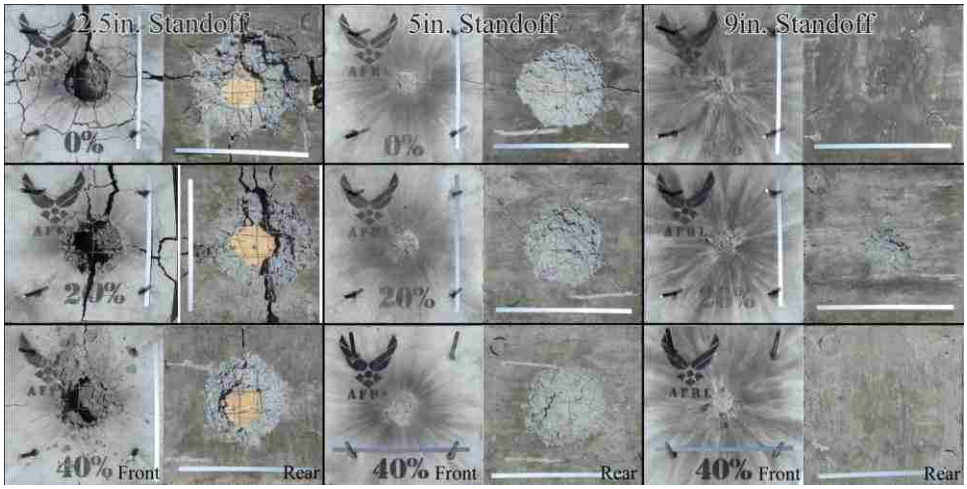

Figure 14: Spall and breach damage to CRC slabs

Table 9: Spall and breach performance (1 in = 2.54 cm)								
Coarse Aggregate Replacement	Standoff [in.]	Front Face Crater Dia. [in.]	Front Face Breach Dia. [in.]	Protected Face Breach Dia. [in.]	Protected Face Spall Dia. [in.]	Protected Face Depth of Spall [in.]	Expected Result (UFC)	Actual Result
40%	2.5	17.875	11.750	11.750	23.125	N.A.	Spall	Breach
20%	2.5	16.969	11.750	11.750	25.500	N.A.	Spall	Breach
0%	2.5	16.719	12.375	12.375	29.000	N.A.	No Damage	Breach
40%	5	6.906	0.000	0.000	21.000	4.750	Spall	Spall
20%	5	6.250	0.000	0.000	21.031	4.125	Spall	Spall
0%	5	5.750	0.000	0.000	22.625	3.625	No Damage	Spall
40%	9	5.813	0.000	0.000	1.000	0	Spall	No Damage
20%	9	6.219	0.000	0.000	11.719	2.250	Spall	Spall
0%	9	4.625	0.000	0.000	1.625	0	No Damage	No Damage

3.2.3 Expected Results Based on Predictor Methods

Expected spall and breach thresholds are calculated in accordance with the UFC 3-340-02 [2008]. Both thresholds are determined with respect to a spall parameter, Ψ, calculated using *Equation 9.* For an uncased charge, the spall parameter is related to standoff distance, R (ft), concrete compressive strength, f'_c (psi), and adjusted charge weight, W_{adj} (lbs). Adjustments are made for burst type, free air or surface burst, as well as shape of explosive.

$$\Psi = R^{0.926} * f'_c{}^{-0.353} * W_{adj}{}^{-.0353} \qquad \textit{Equation 9}$$

The spall and breach thresholds can be computed in accordance with *Equation 10 and Equation 11*, respectively. Both relationships are defined relative to the spall parameter, Ψ, and the ratio of specimen thickness, h, and standoff distance, R.

$$\frac{h}{R} = \frac{1}{-0.02511 + 0.01004 * \Psi^{2.5} + 0.13613 * \Psi^{0.5}} \qquad \textit{Equation 10}$$

$$\frac{h}{R} = \frac{1}{0.028205 + 0.144308 * \Psi + 0.049265 * \Psi^{2}} \qquad \textit{Equation 11}$$

The measured experimental results are presented relative to the UFC formulations for spall and breach in Figure 15. The expected and actual results are also summarized in Table 9 for all cases.

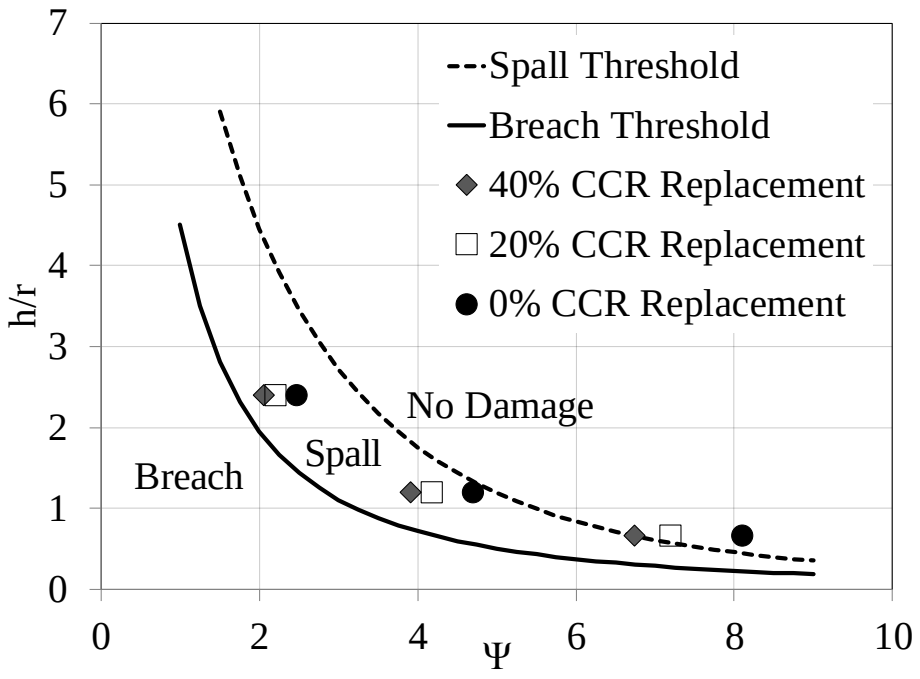

Figure 15: Expected and Actual Results for Spall and Breach

The estimated performance was unconservative for the close-in detonations. For the 2.5 in. standoff the UFC formulations predict spall however all panels resulted in breach. The front face crater diameter was larger and the breach and protected face spall diameter were smaller as rubber replacement was increased. For the standoff of 5 in, the experimental results on the CRC panels agreed with the predicted results. Again the protected interior face damage decreased and the exterior damage increased with additions of rubber.

Overall the spall and breach response observed were inconsistent. This is likely due to the small sample size. Nevertheless, the small study illustrates that although the compressive and tensile strength of the crumb rubber concrete are less than that of normal concrete, they have similar resistance against near field blast demands. Given the lighter unit weight and lower strength of the crumb rubber concrete, energy dissipation enhancement must be inherent in CRC to result in similar performance.

3.3 Ballistic penetration of CRC

High velocity impact of primary fragments represents an important safety concern for building occupants. Primary fragments are formed with the detonation of cased explosives. These fragments are small in size and travel at velocities of several thousand feet per second. Because of their small size and high velocities, primary fragments can have detrimental effects on barriers. If fragments have enough energy, they can penetrate barriers, cause spalling on the interior face, or pass through (perforate). Fragments passing through and spall caused by fragments present a danger to occupants of the structure. [UFC 3-340-02 2008]

The ballistic capacity of CRC was assessed to evaluate if the penetration resistance of concrete is enhanced by the addition of crumb rubber aggregate. The resistance was examined by firing Fragment Simulating Projectiles (FSPs) at increasing velocities into 6 in (150 mm) thick panels. The depth of penetration (DOP) in the panels was measured. The ballistic resistance characteristics were compared to the performance of traditional concretes as predicted by three approaches. The approaches include the UFC 3-340-02 [2008], National Defense Research Committee (NDRC) [Kennedy, 1976], and Haldar [1984].

3.3.1 Penetration Experiment Design

In the DOP study three mix designs were examined: a 10%, 20%, and 40% coarse aggregate replacement. For each of the three designs a constant fine aggregate replacement of 10% is used. The compressive and tensile strengths of the materials were measured. The material strengths are summarized in Table 1. As discussed previously, the concrete strengths decrease with higher additions of rubber aggregate.

A fragment simulating projectile (FSP) was used for the ballistic study to examine the resistance against mortar and rocket fragments. A 207 grain FSP (Figure 16a) was determined to best represent the munitions and was chosen as the design fragment. The FSPs were shot with a powder actuated 50 caliber 36 in. universal receiver (Figure 16b). The FSP impact velocity ranged from 1258 to 3680 ft/sec (383 to 1122 m/sec). The specimens were evaluated in an environmentally controlled room maintained at approximately 50% relative humidity and 77° F (25° C) temperature. The impact

velocities of the projectiles were measured using Oehler Model 35P chronographs with Oehler Model 57 infrared light screens.

The setup is illustrated in Figure 16 b and c. A 6 in (150 mm) thick panel size was chosen to prevent complete penetration of the fragments. The crater diameter was measured on the face of the specimen to the outermost region of the crater (Figure 16d). Three measurements were taken diagonally across the crater zone and averaged. The depth of penetration of the fragment was measured by placing a straight edge across the face and measuring the largest depth of the impact crater (Figure 16e). In some cases the fragment was embedded in the specimen. For these cases the fragment was removed and the depth to the bottom of the impact crater was taken.

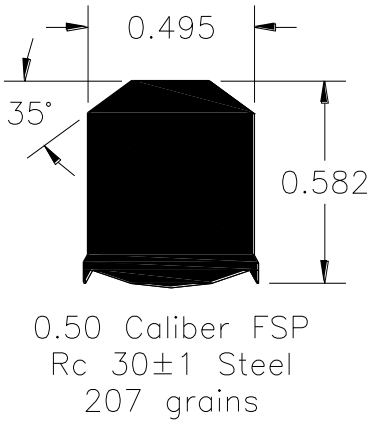

a) Design Fragment Simulating Projectile

b) Ballistic Range

c) Specimen Support

d) Crater Measurement

e) Depth Measurement

Figure 16: Ballistic range and setup (1 in = 2.54 cm)

3.3.2 Experimental Results of Depth of Penetration Evaluation

The impact velocity, front side crater diameter, and depth of penetration were measured for each impact. The impact shape and sizes are illustrated in Figure 17. The results are

graphically illustrated in Figure 18. As illustrated increasing quantity of rubber replacement resulted in smaller crater size and greater depth of penetration.

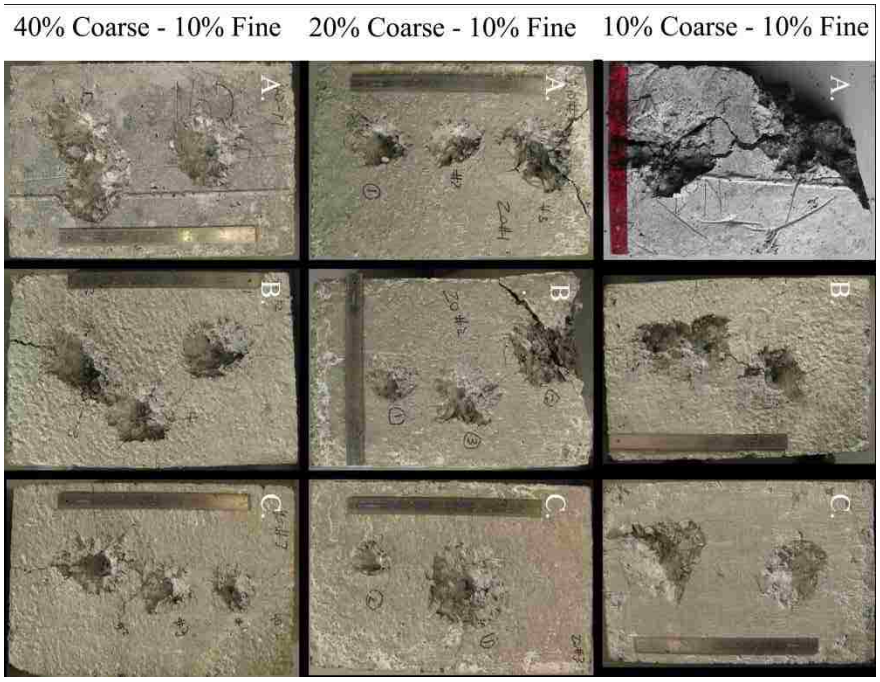

Figure 17 : Depth of Penetration Damage

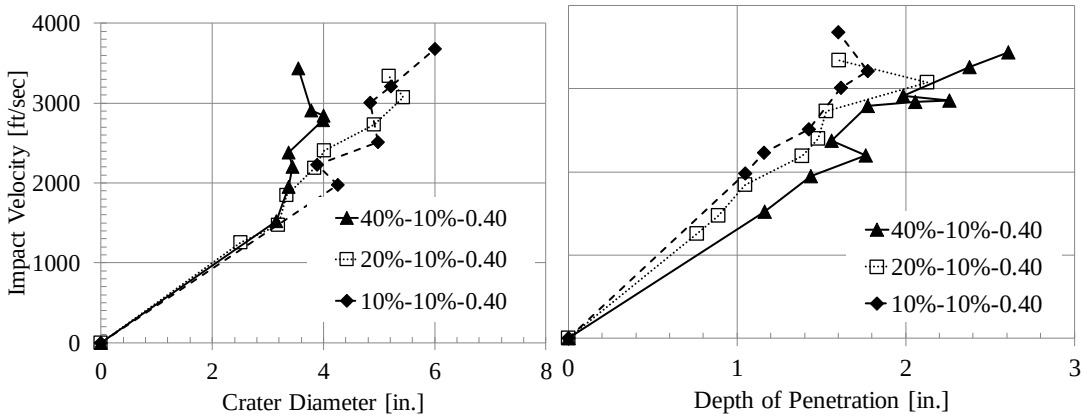

Figure 18: Penetration diameter and depth of crumb rubber concrete (1 in = 2.54 cm, 1 ft/sec = .205 m/sec)

3.3.3 Expected Results Based on Predictor Method

The depth of penetration measured was compared with predictor methods. Three predictive methods were used, the UFC 3-340-02, modified NDRC, and Haldar. Numerous formulae have been formulated to deal with depth of penetration. The equations used represent three empirical formulae that are considered applicable today. [Bangash 2006] Each equation relates the depth of penetration, X_f (in.), to the fragment velocity, V_s (fps), concrete compressive strength, $f'c$ (psi), fragment weight, W_f (lbf), fragment diameter, d (in.), and a nose shape factor, N. A nose shape factor of 0.918 was used as a conservative approximation of the fragment o-give.

The UFC (3-340-02 2008) prediction, *Equation 12* and *Equation 13*, includes two different equations depending on the ratio of the depth of penetration to the fragment diameter.

$$X_f = 4.0x10^{-3}\left(\frac{12.91}{f'c^{0.5}} N \frac{16W_f}{d^3}\right)^{0.5} d^{1.1} V_s^{0.9} \rightarrow X_f \leq 2d \quad \textit{Equation 12}$$

$$X_f = 4.0x10^{-6} \frac{12.91}{f'c^{0.5}} N \frac{16W_f}{d^3} d^{1.2} V_s^{1.8} + d \rightarrow X_f \geq 2d \quad \textit{Equation 13}$$

The modified NDRC prediction, *Equation 14* and *Equation 15*, similarly includes two equations [Kennedy, 1976].

$$X_f = 2d^{0.5}\left(\frac{180}{f'c^{0.5}} NW_f\right)^{0.5}\left(\frac{V}{1000d}\right)^{0.9} \rightarrow X_f \leq 2d \quad \textit{Equation 14}$$

$$X_f = \frac{180}{f'c^{0.5}} NW_f \left(\frac{V}{1000d} \right)^{1.8} + d \rightarrow X_f \geq 2d \qquad \textit{Equation 15}$$

The Haldar prediction, *Equation 17*, *Equation 18*, and *Equation 19*, includes three equations depending on the impact factor, *I*, as defined in *Equation 16* [Haldar, 1984].

$$I = \frac{W_f N V_s^{\,2}}{32.2 d^3 f'c} \qquad \textit{Equation 16}$$

$$X_f = d(-0.0308 + 0.2251I) \rightarrow 0.3 \leq I \leq 4.0 \qquad \textit{Equation 17}$$

$$X_f = d(0.6740 + 0.0567I) \rightarrow 4.0 \leq I \leq 21.0 \qquad \textit{Equation 18}$$

$$X_f = d(1.1875 + 0.0299I) \rightarrow 21.0 \leq I \leq 455.0 \qquad \textit{Equation 19}$$

The comparison between the experimental results and the UFC, modified NDRC, and Haldar predictions are shown in Figure 19 for the 10%, 20% and 40% coarse aggregate replacement levels.

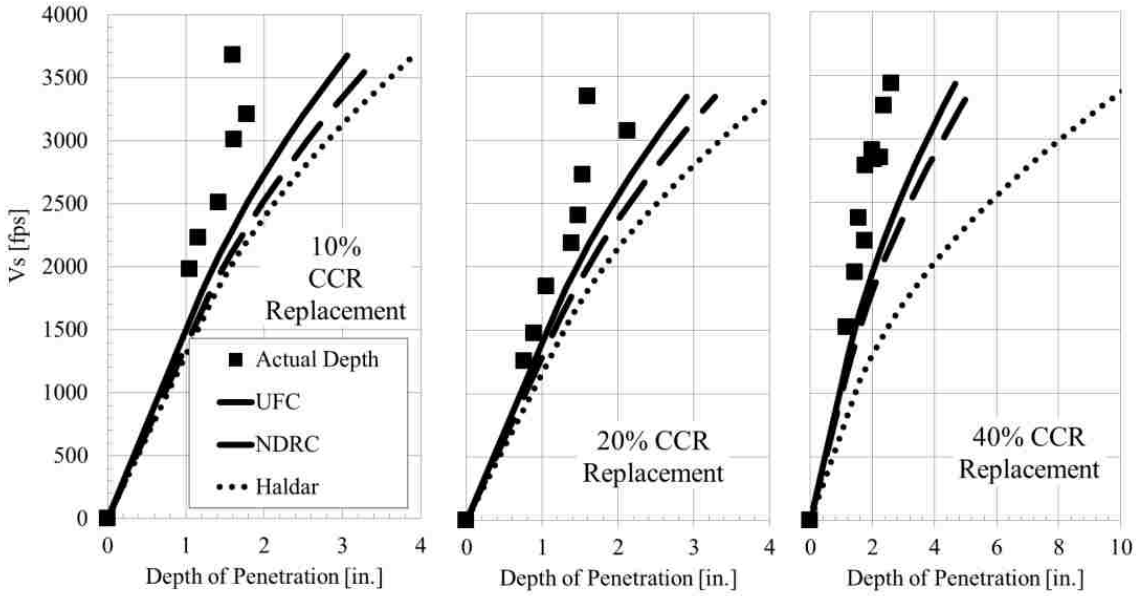

Figure 19: Depth of Penetration Comparison with Predictor Methods (1 in = 2.54 cm, 1 ft/sec = .305 m/sec)

The Haldar, UFC, and NDRC methods provide a conservative estimation of depth of penetration. All three prediction methods were more accurate at lower fragment velocities. The percent error was calculated comparing the actual results and those predicted by the NDRC equation (NDRC was used because it gave the nearest approximation). The average percent error for the 10%, 20%, and 40% coarse replacement is 28.72%, 22.13%, and 37.13% respectively. Although the panels with more CRC resulted in a greater depth of penetration, the difference between the experimental depth and predicted depth was greater for higher levels of CRC. This result suggests that the rubber has some characteristics that increase ballistic capacity.

As discussed previously, an increase in crumb rubber decreases the density of the concrete. For a given weight, a CRC specimen would have more thickness then a

concrete specimen without rubber. Clearly, this increased thickness would have a positive effect on the ballistic capacity of the specimen. The additional thickness would not change the depth of penetration as calculated above, however the additional thickness represents additional depth the fragment must penetrate to break through the specimen. In this way, when weight is the normalizing factor, a CRC specimen has improved ballistic resistance over conventional concrete.

3.4 Ballistic Perforation of CRC

The ballistic perforation of CRC was examined in accordance with the Department of Defense Test Method Standard V_{50} Ballistic Test For Armor [DoD 1997]. The method determines the velocity, V_{50}, at which a given fragment will penetrate armor 50% of the time. The perforation resistance characteristics were compared to the performance of traditional concretes as predicted by the UFC 3-340-02 [2008].

3.4.1 Perforation Test

For the V_{50} study 20% and 40% coarse aggregate replacements are compared with a 0% replacement control. The control is tested at two ages to examine the resistance at a low and high compressive strength. The panels used for the ballistic study do not include fine rubber aggregate. The material strengths are summarized in Table 1.

As with the DOP study previously described, the performance is assessed relative to a 207 grain FSP. Two panel thicknesses, 2 in. and 3 in. (50.8 mm, 76.2 mm), were examined for the study. The surface of the panels measured 2 ft (0.61 m) tall by 1.5 ft

(0.46 m) wide. Several panels were fabricated for each mix design to provide enough samples to adequately determine one V_{50} point.

The V_{50} velocity was determined by taking the average of an equal number of highest partial penetration velocities and the lowest complete penetration velocities which occur within a specified velocity spread. Four shots with a velocity spread of 60 fps (18.3 m/sec) or six shots with a velocity spread of 90 fps (27.4 m/sec) were used to determine V_{50}. Complete penetration occurs when the fragment or pieces of the panel are ejected from the protected face and result in perforation of a witness panel located 6.5 in. (165.1 mm) from the rear of the specimen. Perforation was determined by holding up the panel to a 60 Watt bulb and inspecting for light passage. The witness panel consisted of a 0.020 in. (0.51 mm) thick sheet of 2024 T3 aluminum. Partial penetration refers to anything less than complete penetration. All tests were conducted in an environmentally controlled testing facility. The average condition at time of testing was 77ºF and 47% relative humidity.

3.4.2 Results of V_{50} Study

The measured V_{50} for the four concrete mixes are summarized in Table 10. The results are presented graphically in Figure 20. The V_{50} is presented relative to the panel thickness and areal density. The areal density is a measure of weight of the panel per unit surface area. This measure is often used to compare the ballistic efficiency of the system with alternate materials.

Table 10: V_{50} results

Coarse Aggregate Replacement [%]	Panel Thickness [in. (cm)]	Areal Density [lb/sq.ft. (kPa)]	Est. Compressive Strength [psi (MPa)]	V_{50} [ft/sec (m/s)]	Expected Velocity [ft/sec, (m/s)]
40%	3 (7.62)	32.24 (1.548)	2610 (17.99)	2818 (859)	2161 (659)
40%	2 (5.08)	20.94 (1.003)	2610 (17.99)	1601 (488)	1086 (331)
20%	3 (7.62)	34.31 (1.643)	5107 (35.21)	2811 (857)	2603 (793)
20%	2 (5.08)	21.85 (1.046)	5093 (35.11)	1561 (478)	1308 (399)
0%	3 (7.62)	37.36 (1.789)	8195 (56.50)	3118 (950)	2970 (905)
0%	2 (5.08)	24.32 (1.164)	8195 (56.50)	1753 (534)	1493 (455)
0%	3 (7.62)	37.79 (1.809)	3365 (23.20)	3315 (1010)	2319 (707)
0%	2 (5.08)	24.67 (1.181)	3365 (23.20)	1641 (500)	1166 (355)

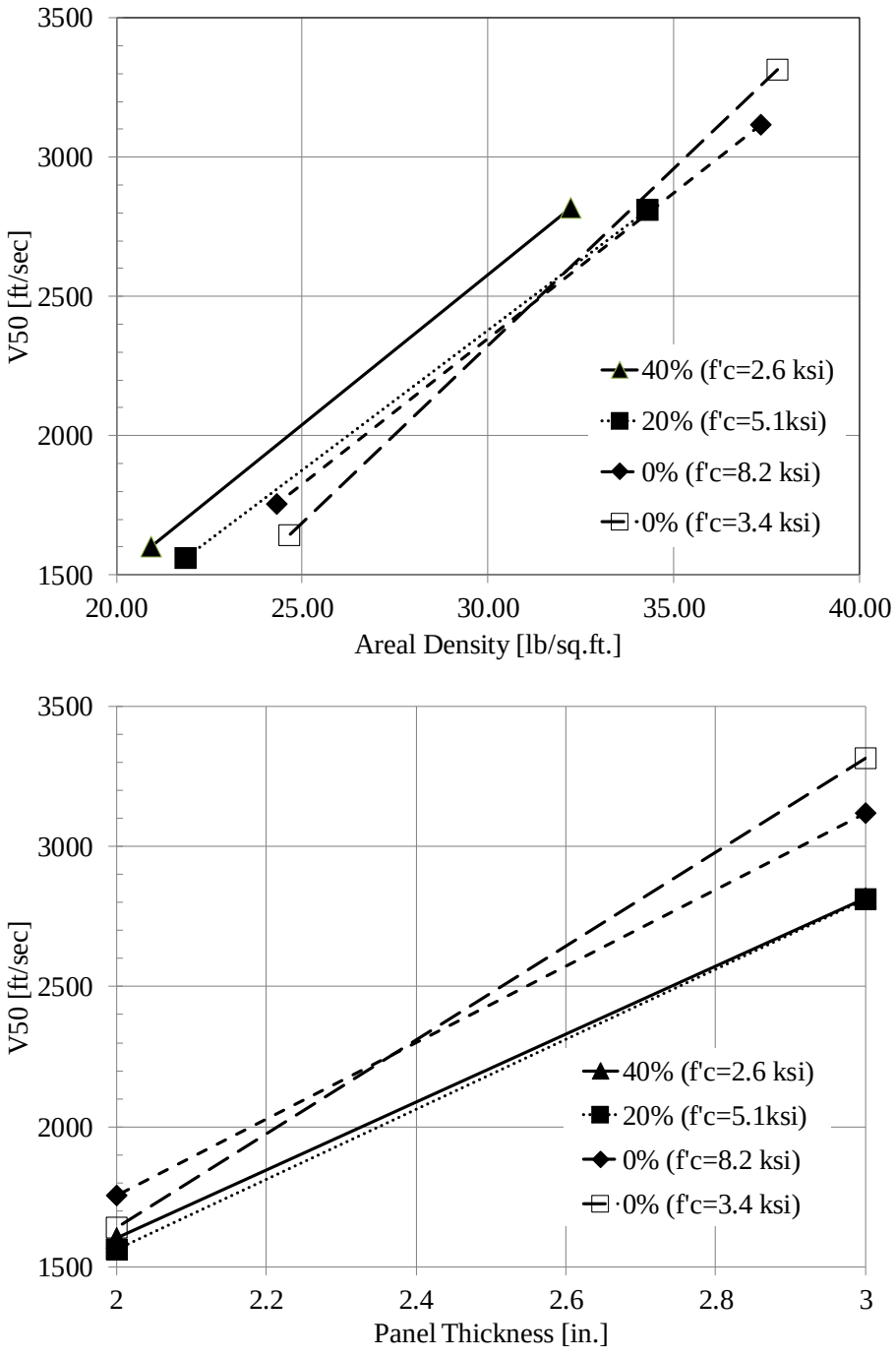

Figure 20: Ballistic resistance of crumb rubber concrete

3.4.3 Estimated Ballistic Penetration Resistance

The perforation resistance of the panels are compared to UFC 3-340-02 [DoD 2008] predictions. Perforation thickness of a given concrete type is computed from the depth of penetration calculations previously conducted. The minimum concrete thickness to prevent perforation, T_{pf}, is presented in *Equation 20.* It is based on the corrected depth of penetration, X_f, as found by *Equations 12 and 13* and the fragment diameter, d.

$$T_{pf} = 1.13 X_f d^{0.1} + 1.311 d \qquad \textit{Equation 20}$$

The fragment velocities at which the 2 and 3 in. thick panels would be sufficient to prevent perforation were calculated with Equations 12, 4, and 5. The results are found in Table 10. Figure 21 presents a comparison between the expected results from equation 9 and the experimental V_{50} results.

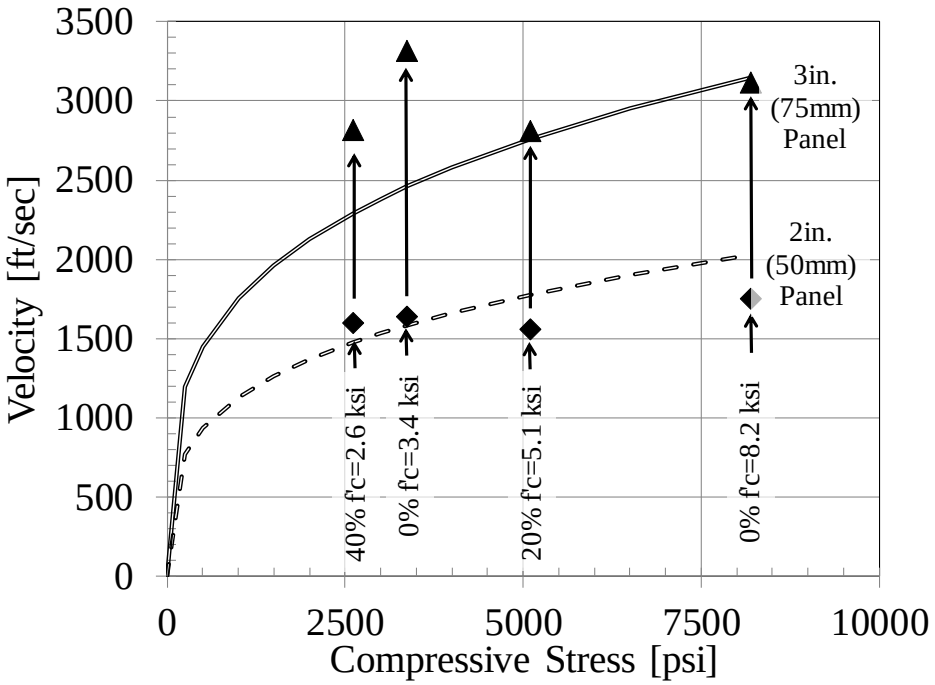

Figure 21: V_{50} expected and actual results

The use of crumb rubber decreases the ballistic stopping capability when compared to an equivalent thickness of conventional concrete as illustrated in Figure 20. However when weight is a limiting factor, CRC exhibits an improvement over conventional concrete. The unit weight of CRC is lower than standard concrete. When comparing the ballistic resistance to the areal density, Figure 20 indicates that CRC exhibits an improvement over conventional concrete.

The comparison between the experimental results and expected results based on published equations indicates that standard equations are fairly accurate, though the UFC equation overestimates the effects of compressive strength. The percent error was calculated comparing the actual results and those predicted by the UFC equation. The average percent error for the 0% (*f'c* of 8195 psi), 20% (*f'c* of 5100 psi), 0% (*f'c* of 3365

psi), and 40% (*f'c* of 2610 psi) coarse replacement is -7.24%, -5.16%, 19.23%, and 15.76% respectively. The difference between expected and actual is small for the panels with higher compressive strength. The equation is also unconservative for the high compressive strengths. The accuracy of the equation for low compressive strengths is much lower, though it is conservative. The UFC equations are less accurate for increasing levels of CRC replacement, however it appears that the cause of the poor accuracy is the low level of compressive strength as opposed to the ballistic resistance of the CRC. However, independent of the cause, the use of CRC does not decrease the perforation resistance as much as is expected by the equations in the UFC.

3.5 Conclusions

Research has shown that Portland cement concrete utilizing shredded vehicle tires for a partial aggregate replacement is effective in providing energy absorbing enhancements. To examine if these capabilities are useful for military applications crumb rubber concrete is examined against blast and ballistic demands. CRC is studied for spall and breach resistance against near field detonation of high explosives and ballistic penetration and perforation resistance against small mass fragments. The effectiveness of CRC is compared to control concrete mixes and to predictive formulations. The results of the study are summarized as follows:

3.5.1 Spall and Breach Resistance

- The results indicate that an increase in rubber replacement results in an increase in the crater diameter and depth of spall on the exterior face and a decrease in the breach and spall diameter on the protected face.
- The UFC spall and breach predictive equations were unconservative in four of the nine close-in detonations conducted.
- While additional tests may be warranted to assess the reproducibility of the results, the improvements in spall and breach resistance provided by CRC was minimal.

3.5.2 Ballistic Penetration Resistance

- Ballistic penetration tests using a 207 grain FSP indicates that an increase in rubber coarse aggregate reduces the ballistic resistance of concrete. Increases in the depth of penetration were observed for higher rubber replacements and were attributed to the corresponding reduction in concrete compressive strength.
- Three methods for predicting depth of penetration were examined. All three methods gave conservative results for all data points collected. The NDRC method provides the nearest prediction to the actual results followed by the UFC and Haldar methods.
- All three prediction methods showed improved accuracy at lower impact velocities. Although the panels with more CRC resulted in a greater depth of penetration, the difference between the experimental depth and predicted depth was greater for higher levels of CRC. This result suggests that the rubber has some characteristics that increase ballistic capacity.

3.5.3 Ballistic Perforation Resistance

- The use of crumb rubber decreases the ballistic stopping capability when compared to an equivalent thickness of conventional concrete.
- When comparing the ballistic resistance to the areal density, CRC exhibits an improvement over conventional concrete.
- The comparison between the experimental results and expected results based on published equations indicates that standard equations are conservative for lower levels of compressive stress. This means that the use of CRC does not decrease the perforation resistance as much as is expected by the equations in the UFC.

The results indicate that CRC replacement decreases the resistance of concrete to brittle mode response for blast design. However, comparison with predictor equations suggests that the decrease is less than what might be expected from concrete with similar compressive strength. That is, although the addition of CRC to concrete decreases the compressive strength of the concrete, it decreases the brittle mode blast resistance less. The addition of crumb rubber does increase the brittle mode failure blast resistance just not enough to outweigh the accompanying decrease in compressive and tensile strength of the concrete.

The ballistic resistance of CRC shows an interesting trend when examined as a function of unit weight. Traditionally rubber aggregate is included as a volume replacement of standard concrete coarse aggregate. Consequently, the resulting unit weight of CRC is lower than standard concrete. The improvement in ballistic capability relative to areal density indicates that CRC may be advantageous when weight is an issue. The relative

weight of the material needed to stop a particular threat is lower than that of conventional concrete.

It is important to consider that the improvement is provided even though the material strength is considerably lower. To achieve comparable ballistic resistance with a considerably lower strength indicates that the rubber provides some damping enhancements when ballistic impacts are a concern. It is possible that with appropriate choices of rubber constitutive properties and gradation, further enhancements can be achieved. Further study of the ballistic properties is warranted.

Chapter 4: Spall and Breach of a Concrete Panel in LS-Dyna

A finite element model of the spall and breach test from section 3.2 was completed in the finite element program LS-Dyna. Models were completed for only the 0% rubber replacement members and were completed for the 2.5in, 5in, and 9in standoff distances. The finite elements models were made to compare the experimental results and the expectations that were calculated using the UFC equations. The reliability of these findings may be validated further using a finite element model. The model also offers an opportunity to examine the effectiveness of LS-Dyna for such brittle mode response blast load problems such as the one being tested.

4.1 Model Overview

The Concrete panel geometry was modeled as a 3-Dimensional box with dimensions matching the experimental members, 42 in. x 42 in. x 6 in.. The model was generated with 0.5 in. cubic elements. The cubic elements chosen were constant stress solid elements with nodes at the corners and 6 DOF per node. This geometry results in a model that includes 84,672 elements, 93,925 nodes, and 563,550 DOF. Figure 22 depicts the basic model in the LS-Dyna interface.

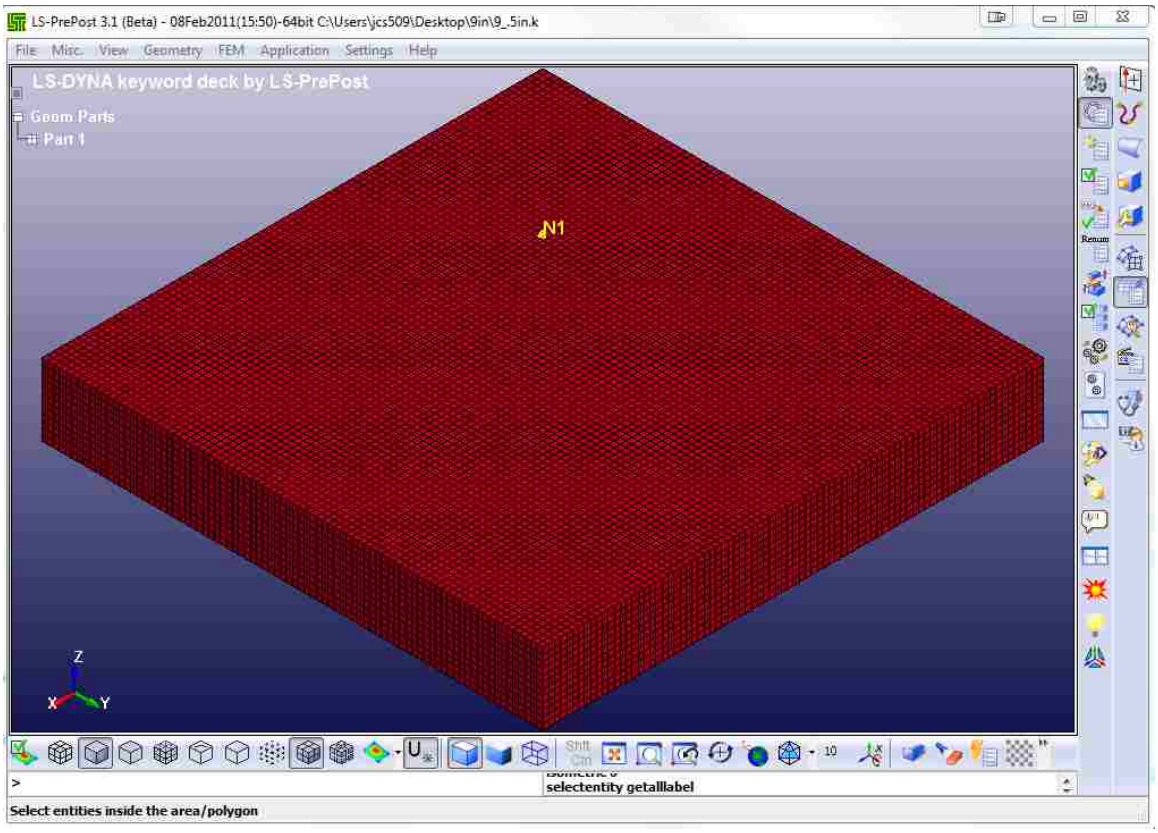

Figure 22: LS-Dyna Concrete Panel Model

The boundary conditions were chosen to resemble those of the experiment. Translation in the vertical direction was supported at every node along the bottom edge. The experiment did not include any secure horizontal supports, however friction was sufficient to hold the panels in place during the experiment. For this reason, to prevent free motion horizontally, the x direction of displacement was supported at every node along one edge, and the y direction of displacement was supported at every node along an adjacent edge. This introduces a lack of symmetry into the model, but that is acceptable for a basic spall and breach model.

The material that was used to model concrete in LS-Dyna is Material 159 – CSCM Concrete. CSCM Concrete requires input values for compressive strength, f'c, maximum aggregate size, and mass density. Values entered were f'c = 5559 psi, maximum aggregate size of 0.75in, and mass density of 0.087 lbs / $in.^3$. The CSCM concrete material uses these three input values to find all other necessary values such as tensile strength and modulus of elasticity. A more comprehensive material exists in LS-Dyna that allows the user to enter values for these properties as well as many others, however for this initial investigation it was decided that the standard CSCM Concrete material would be sufficient.

Additionally the material model includes an "ERODE" option. Erode causes elements to lose all stiffness and strength after a threshold amount of damage is achieved. Both brittle (tensile) and ductile (compressive) damage is considered for the erode option. An element erodes if the accumulated damage parameter exceeds 0.99 and a maximum principal strain value is exceeded. To simplify the evaluation an erode value of 1.00 is used in the analysis. For this case the max principal strain check is not used and instead the elements erode when the damage parameter exceeds 0.99. Eroded elements for the spall and breach case that was tested would represent the area of spall/breach. In this way the model does not show the spalled concrete detach from the member at some velocity, but rather just shows the damage crater that exists after spall occurs.

The experimental model includes a small amount of rebar. The rebar included in the experiment to prevent temperature or shrinkage damage to the panels prior to testing. The effects of the rebar on the capacity of the concrete to withstand the blast without

spall or breach was considered negligible in the experiment. For this reason no rebar was included in the finite element model.

The load caused by the 2 lb C-4 detonation was modeled in LS-Dyna using the Blast Load function. The Blast Load function allows the user to input the equivalent TNT mass of the charge, and the location of the charge. Using this information the pressure load on the chosen member face is applied directly. The input for this model was equivalent mass equal to 0.00622 dozens of slugs, and at three locations: 2.5 in., 5 in., and 9 in. away from the face of the member in the vertical direction and centered on the panel horizontally.

4.2 Model Results

Time history data was produced from the model for the three standoff distances. Data was taken every 0.001 seconds until a time of 0.1 second. The spall occurred within the first 0.01 seconds for each model. The results are illustrated in Figure 23 and Table 11 . These results are taken at a time of 0.1 seconds after detonation, and show the erosion damage of the panels.

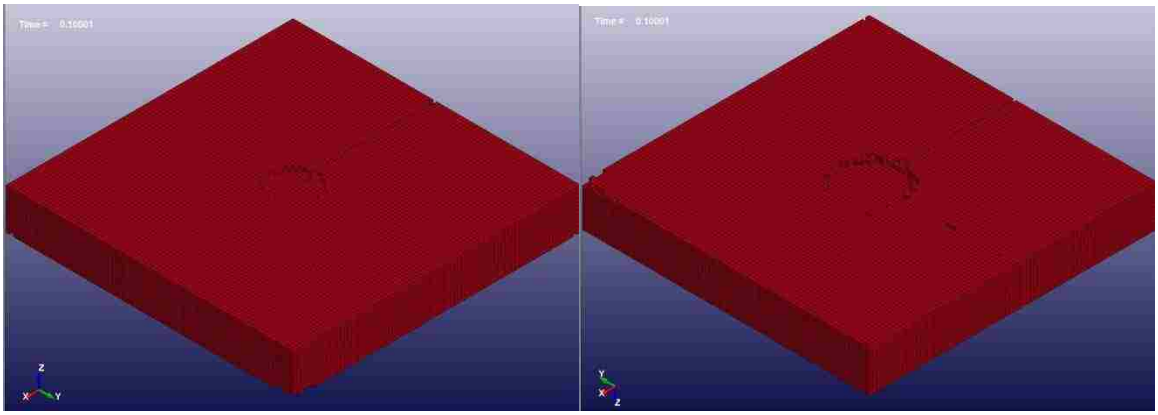

Top **Bottom**

A) 2.5 in Standoff

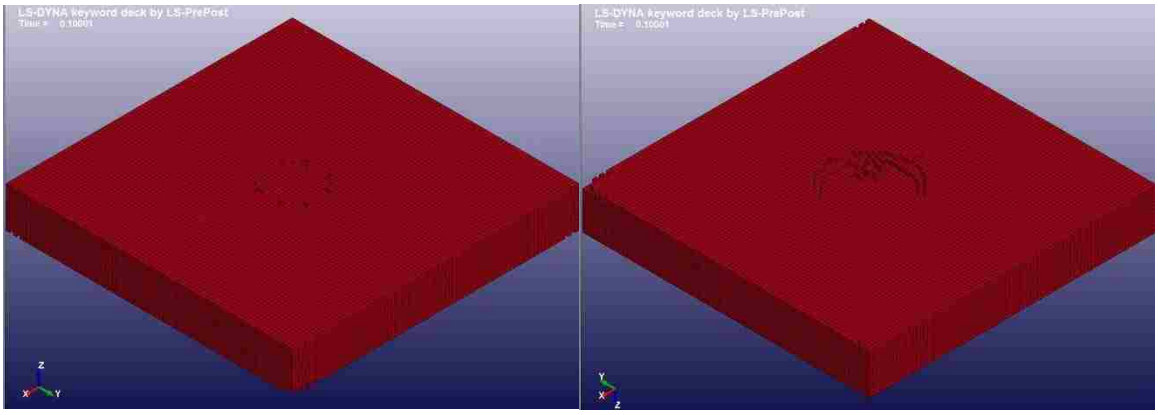

Top **Bottom**

B) 5in Standoff

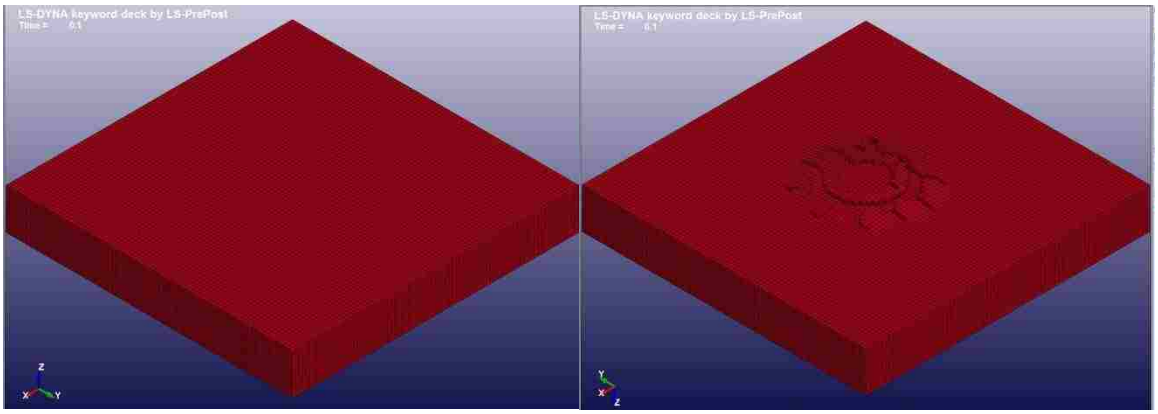

Top **Bottom**

C) 9in Standoff

Figure 23: LS-Dyna Spall Erosion Results

Table 11: Spall and breach performance (1 in = 2.54 cm)

	Experimental				LS-Dyna Model				
Standoff [in.]	Front Face Crater Dia. [in.]	Protected Face Spall Dia. [in.]	Protected Face Depth of Spall [in.]	Result	Front Face Crater Dia. [in.]	Protected Face Spall Dia. [in.]	Protected Face Depth of Spall [in.]	Interior Damage Diameter [in.]	Result
2.5	16.719	29.000	Breach	Breach	7	10	1.5	18	Spall
5	5.750	22.625	3.625	Spall	NA	12	1.5	21	Spall
9	4.625	1.625	0	No Damage	NA	11	1	20	Spall

The results indicate that spall occurred on the panel for each standoff distance. The depth of the spall increased as the standoff distance became smaller in the three models. The model that included the 9in standoff did not include damage on the front face. The other two models included damage on the front face and the model with a 2.5 in standoff clearly showed more damage to the front face than the model with the 5 in standoff (limited damage with no crater). The spall diameters and interior damage diameters did not show a significant trend. For all three tests these two properties were clumped around 10 in and 20 in respectively.

4.3 Conclusions

The results of the finite element analysis are on the same order as the results found from experimentation and those found from the UFC equations. Although the results are not matched exactly, certain trends that were expected occurred in the finite element model.

Front face damage was clearly more likely for closer standoff distances as expected. Spall depth damage was larger for a closer standoff distance as well. However, the spall diameter and interior damage data found does not agree with what was expected. Clearly there is room for improvement with the finite element model.

From the given model it is not clear how the blast load is applied to the panel. The way the blast load is modeled may not be accurate for all loading scenarios such as this one with such a close-in blast. Also the way the erosion works may have introduced error in to the model. A large amount of interior damage was found in the model causing erosion of interior elements. Although failure stress may have occurred on the interior of the actual experimental elements, the same type of erosion does not occur. This likely had a significant effect on the spall diameters and any damage that did not occur at the time of first damage.

The variability that exists in spall and breach testing and calculations makes it unlikely that a finite element model would exactly match results found from an experiment, but the results are on the same order and show many similarities. More work should be done, specifically focusing on the material erosion and application of the blast load, however the early finite element results are promising.

References

ACI Committee 209, “Prediction of Creep, Shrinkage, and Temperature Effects in Concrete Structures,” ACI 209R-92, American Concrete Institute, Farmington Hills, MI, Reapproved 1997, 47 pp.

ACI Committee 318, “Building Code Requirements For Structural Concrete (ACI 318-08) and Commentary,” American Concrete Institute, Farmington Hills, MI, 2008, 468 pp.

ASTM Standard A185, 2007, “Standard Specification for Steel Welded Wire Reinforcement, Plain, for Concrete,” ASTM International, West Conshohocken, PA, 2007, DOI: 10.1520/A0185_A0185M-07, www.astm.org.

ASTM Standard C31, 2005, “Standard Practice for Making and Curing Concrete Test Specimens in the Field,” ASTM International, West Conshohocken, PA, 2009, DOI: 10.1520/C0031_C0031M-09, www.astm.org.

ASTM Standard C33, 2001, “Standard Specification for Concrete Aggregate,” ASTM International, West Conshohocken, PA, 2001, DOI: 10.1520/C0033-01, www.astm.org.

ASTM Standard C39, 2005, "Standard Test Method for Compressive Strength of Cylindrical Concrete Specimens," ASTM International, West Conshohocken, PA, 2005, DOI: 10.1520/C0039_C0039M-05E01, www.astm.org.

ASTM Standard C78, 2009, " Standard Test Method for Flexural Strength of Concrete (Using Simple Beam with Third-Point Loading)," ASTM International, West Conshohocken, PA, 2009, DOI: 10.1520/C0078-09, www.astm.org.

ASTM Standard C192, 2007, "Standard Practice for Making and Curing Concrete Test Specimens in the Laboratory," ASTM International, West Conshohocken, PA, 2007, DOI: 10.1520/C0192_C0192M-07, www.astm.org.

ASTM Standard C231, 2009, "Standard Test Method for Air Content of Freshly Mixed Concrete by the Pressure Method," ASTM International, West Conshohocken, PA, 2009, DOI: 10.1520/C0231-09A, www.astm.org.

ASTM Standard C469, 2002, "Standard Test Method for Static Modulus of Elasticity and Poisson's Ratio of Concrete in Compression," ASTM International, West Conshohocken, PA, 2002, DOI: 10.1520/C0469-02E01, www.astm.org.

ASTM Standard C496, 2004, " Standard Test Method for Splitting Tensile Strength of Cylindrical Concrete Specimens," ASTM International, West Conshohocken, PA, 2004, DOI: 10.1520/C0496_C0496M-04E01, www.astm.org.

Bangash, M.Y.H., and Bangash, T. 2006. Explosion-Resistant Buldings. London, UK: Springer-Verlag.

Bewick, B., Salim, H., Saucier, A., and Jackson, C., "Crumb Rubber-Concrete Panels under Blast Loads," Air Force Research Laboratory Report, AFRL-RX-TY-TP-2010-0052, May 2010.

Biggs, J. M. 1964. Introduction to Structural Dynamics. New York, NY: McGraw-Hill Book Company Inc.

Coughlin, A.M., Musselman, E.S., Schokker, A.J., Linzell, D.G., "Behavior of Portable Fiber Reinforced Concrete Vehicle Barriers Subject to Blasts from Contact Charges," International Journal of Impact Engineering, Vol 37, pp. 521-529, Aug. 2009.

Department of Defense USA, "V_{50} Ballistic Test for Armor", Army Research Laboratory, Weapons and Materials Research Directorate, MIL-STD-662F, December 1997.

Department of Defense USA, "Unified Facilities Criteria: Structures to Resist the Effects of Accidental Explosions," UFC 3-340-02, December, 2008.

Eldin, Neil N., and Senouci, Ahmed B., "Rubber-Tire Particles as Concrete Aggregate," Journal of Materials in Civil Engineering, Vol. 5, No. 4, pp. 478-496, Nov. 1993

Eldin, Neil N., and Piekarski, Julian A. (1993). "Scrap Tires: Management and Economics," Journal of Environmental Engineering, Vol. 119, No. 6, pp. 1217-1232, Nov./ Dec. 1993

Epps, J. A. (1994). ''Uses of recycled rubber tires in highways.'' *Synthesis of highway practice 198*, Transportation Research Board, National Research Council, Washington, D.C.

Haldar, A., and Hamieh, H., "Local Effect of Solid Missiles on Concrete Structures," Journal of Structural Engineering, ASCE, Vol. 110, No. 5, May 1984.

Hognestad, E., "A Study of Combined Bending and Axial Load in Reinforced Concrete Members," University of Illinois Engineering Experimental Station, Bulletin Series No. 399, November 1951, 128 pp.

Kennedy, R. P., "A Review of Procedures for the Analysis and Design of Concrete Structures to Resist Missile Impact Effects," Nuclear Engng and Design, Vol. 37, 183-203 (1976).

Khatib, Zaher K., and Bayomy, Fouad M., "Rubberized Portland Cement Concrete," Journal of Materials in Civil Engineering, Vol. 11, No. 3, pp. 206-213, Aug. 1999

Taha, M. M. Reda, El-Dieb, A. S., Abd El-Wahab, M. A.; and Abdel-Hameed, M. E., "Mechanical, Fracture, and Microstructural Investigations of Rubber Concrete," Journal of Materials in Civil Engineering, Vol. 20, No. 10, pp. 640-649, Oct. 2008

Turatsinze, A., Bonnet, S., and Granju, J.-L., "Mechanical Characterization of Cement-Based Mortar Incorporating Rubber Aggregates from Recycled Worn Tires," Building and Environment, Vol. 40, No. 2, pp. 221-226, Feb. 2005

US Army, "Technical Manual Design and Analysis of Hardened Structures to Conventional Weapons Effects," Army TM5-855-1, Washington DC, 1998.

U.S. Environmental Protection Agency, "Scrap Tires," http://www.epa.gov/osw/conserve/materials/tires/index.htm, Access August 28, 2008.

U.S. EPA, 2008. "Scrap Tires, Common Wastes and Materials," [online]. Available from: http://www.epa.gov/osw/conserve/materials/tires/index.htm [Accessed 24 August 2010].

Wong, Sook-Fun, and Ting, Seng-Kiong, "Use of Recycled Rubber Tires in Normal and High-Strength Concretes," ACI Materials Journal, Vol. 106, No. 4, pp. 325-332, July-August 2009.

Zheng, L., Sharon Huo, X., and Yuan, Y., "Strength, Modulus of Elasticity, and Brittleness Index of Rubberized Concrete," Journal of Materials in Civil Engineering, Vol. 20, No. 11, pp. 692-699, Nov. 2008.

Vita

Joseph Charles States, the son of Stanley and Kathleen States, was born on March 17, 1987 in Pittsburgh, PA. Joseph earned a Bachelor of Science in Civil Engineering from Carnegie Mellon University in May 2009. Joseph began his graduate studies in the Department of Civil and Environmental Engineering at Lehigh University in August 2009. He will receive his Master of Science in Structural Engineering in May 2011.